Transverse Single Spin Asymmetry of Direct Photons in Run15 pp 200 GeV at Midrapidity

Nicole Lewis

March 6, 2020

Contents

List of Figures

List of Tables

1 Analysis Organization

1.1 Location of code and working directories in the RCF

Directory of taxi code:
`offline/AnalysisTrain/Run15ppPhotons`
Taxi macro name:
`Run_Run15ppPhotons.C`
Location of ERT sample taxi output:
`/phenix/spin/phnxsp01/nialewis/taxi/Run15pp200CAnoVTXERTPro104/16058/data`
This includes the aggregated taxi output called AllRuns.root as well as macros for make trees of curated data Location of MB sample taxi output:
`/phenix/spin/phnxsp01/nialewis/taxi/Run15pp200CAnoVTXMBPro104/16056/data/`

Directory for analysis code:
`/direct/phenix+u/workarea/nialewis/Run15ppPhotons/`
The `data` subdirectory includes macros for finding hot towers, calculating the direct photons background and the direct photon cross section. The `simulations` has all code that was use to process single particle Monte Carlos. This includes the modified version of the taxi code called "photons" and subsubdirectories for calculating the background fractions r_{miss} and r_{merge}, as well as the geometric efficiency $C^{geo}_{eff}(p_T)$. All TSSA calculating code is located in the subdirectory `Asymmetry`

Directory for running single particle Monte Carlo simulations:
`/phenix/spin/spin1/phnxsp01/nialewis/dpBackground/`
The subdirectory `oscarFiles` includes the truth single particle files from exodus. The subdirectory `scripts` contains the Condor scripts for running these truth files through PISA and PISAtoDST. The subdirectory `photonsOutput` contains the reconstructed simultions files, the output from once these PISA DST files were runs through the modified version of the Run15ppPhotons taxi code located in
`/direct/phenix+u/workarea/nialewis/Run15ppPhotons/simulations/photons`

1.2 Data Set

This analysis used polarized Run15 $p + p$ data with $\sqrt{s} = 200$ GeV, combining data from all three ERT 4x4 triggers. The taxi code ran over `Run-15 200 GeV p+p (No VTX) pro104 (ERT)` **not** `Run-15 200 GeV p+p pro108 (ERT)` because it has 100 million fewer events. Minimum bias data was also collected in order to calculate the integrated luminosity as well as trigger efficiency for the direct photon cross section cross check. This ran over `Run-15 200 GeV p+p (No VTX) pro104 (MinBias)` **not** `Run-15 200 GeV p+p pro108 (MinBias)` to stay consistent with ERT data.

1.3 Brief Overview of Analysis Steps

This analysis measures the Transverse Single-Spin Asymmetry of direct photons as a function of photon p_T using clusters from the central EMCal. The fill by fill polarization and Gl1P scaler information was also collected for the polarization and relative luminosity corrections. Photon data from two different fills were grouped together to calculate a separate asymmetry for each fill group and p_T bin. To get the final asymmetry value, all 72 fill group asymmetries were averaged together.

These photons were required to pass an isolation cut and also photons that were tagged as coming from either π^0 or η meson decays were eliminated from the direct photon sample. The main source of background for direct photons were the photons that came from $h \to \gamma\gamma$ decays where one of the photons was missed and so they were not eliminated by the tagging cut. This background was calculated using single particle Monte Carlo and treated as a dilution to the asymmetry. Photon merging happens when the photons from a $\pi^0 \to \gamma\gamma$ decay are so close together that the EMCal cannot distinguish them as separate photons. The contribution from merge π^0 decays was found to be small and was added to the over all systematic uncertainty

Systematic studies included bunch shuffling and calculating the direct photon cross section and comparing it to previous PHENIX results $\sqrt{s} = 200$ GeV result PPG136.

2 Physics Motivation

Transverse Single-Spin Asymmetries (TSSAs) are spin-momentum correlation measurements, that measures how the transverse polarization of the nuclear target affects the angular distribution of final state particles. In proton-proton collisions, only one of the protons are transversely polarized and the asymmetry is measured for yields of particles that travel to the left versus the right of the polarized proton going direction. Large forward TSSA in proton-proton collisions have been measured to up to 40%, contradicting the perturbative QCD prediction of less than 1%. Large TSSA were originally discovered in fixed target experiments but have been found to persist in collisions up to $\sqrt{s} = 510$ GeV and transverse momenta up to about 7 GeV, well into the perturbative regime of QCD, and yet their origin remains poorly understood. TSSA measurements have allowed for the development of both transverse momentum dependent and collinear twist-3 descriptions of nonperturbative spin-momentum correlations in the nucleon as well as in the process of hadronization.

Direct photons are uniquely sensitive to initial state effects in proton-proton collisions. Measurements from direct photons are not sensitive to effects from hadronization since they are the only outgoing fundamental particle in QCD 2-to-2 subprocesses. For midrapidity 200 GeV pp collisions, the direct photon cross section is dominated by $q + g \to q + \gamma$ instead of $q + \bar{q} \to g + \gamma$ and so are directly sensitive to gluon spin-momentum correlations in the proton.

3 Analysis Details

The analysis taxi code is located in the directory `offline/AnalysisTrain/Run15ppPhotons` and can be run with the macro `Run_Run15ppPhotons.C`. For this analysis, this code was run over Run-15 200 GeV p+p (No VTX) pro104 (ERT) instead of Run-15 200 GeV p+p pro108 (ERT) because the former had on the order of 100 million more events and this analysis does not use VTX data. Because Norbert Novitzky's $\pi^0 A_N$ analysis (AN1269) was done with the same Run 15 data set, many elements from his analysis work were used as a starting point.

3.1 Run QA

From Run15 A_N of π^0 the following runs were eliminated from the list either because they had a low vertex distribution or low π^0 rate, details can be found in Section 2.4 of AN1269:

422531 422540 432003

These next runs were not used for the asymmetry analysis based of off the Spin DB Run15 quality analysis note, see Section 2.1 of AN1255.

422375 423413 425567 425941 427129 427136 427137 431236

The run below was not used because it was from fill 18717 where the polarization was set to zero because of strange dynmaics in the yellow beam's polarization:

424227

The following runs were not used in asymmetry calculations, because though they contained cluster data, the Gl1P scalers were either zero or very small:

426313 426315 426316 426319 426320 429590 431854

As shown in Figure 5 fills 18777 and 18778 had outlier yellow beam relative luminosity values and thus were eliminated from any asymmetry calculations. This translates to these additional runs being eliminated from the good run list:

426307 426308 426353 426365 426366 426378 426383 426391 426394

The following runs were eliminated because of an analysis that was done in Section 2.1 and Figure 1 of AN1373, that looked at the run by run ERT trigger efficiency for η yields and found that the efficiency was unusually high for Fill 18758, which corresponds to the following runs:

425688 425691 425692 425693 425694

3.2 Data Cuts

The following cuts were placed on events

1. **Trigger:** Each event had to fire the ERTB, ERTA or ERTC triggers. This corresponded to the trigger bits: `"ERT_4x4b"` and `"ERT_4x4a&BBCLL1"` trigger bits for all runs and `"ERT_4x4c&BBCLL1"` for runs up to run 422085 and `"ERT_4x4c&BBCLL1(narrow)"` for runs after 422085.
2. **Vertex:** BBC vertex required to $\mid z_{vtx} \mid \leq 30$ cm. The z_{vtx} is found using PHGlobal::getBbcZVertex().
3. **Crossings:** Clusters that came from unfilled clusters were also eliminated.

Every photon used in this analysis was required to pass the following cuts for clusters in the central EMCal:

1. **Energy range:** $0.5 \leq E_{core} \leq 20.0$ GeV where E_{core} came from emcClusterContent::ecore()
2. **Shower Shape:** emcClusterContent::prob photon() > 0.02 and clusters found in the PbSc sectors were required to have $\chi^2 < 3$ and photons in the PbGl sectors were required to pass a dispersion cut.
3. **Warnmap and Deadmap:** The cluster's center tower could not be in or next to any tower in the emcClusterContent::warnmap() or emcClusterContent::deadmap() lists
4. **Edge Tower Cut:** All clusters that were centered in towers next to the edge of the sector or one over from the edge were eliminated.
5. **3x3 Hot Tower Cut:** Clusters whose center was in or was next to a tower in the recorded hot tower lists were eliminated. There were two separate lists: lowHotTowers.txt for clusters with energy < 5 GeV and highHotTowers.txt for clusters with energy > 5 GeV. Both lists can be found in the `offline/AnalysisTrain/Run15ppPhotons` directory and the process for finding these hot tower lists is detailed in Section 2.2 of AN1373.
6. **Time of Flight:** $|TOF| < 5$ ns. The TOF was recalibrated using Norbert Novitzky's TOF recalibrator which is described in Section 3.2 of AN1269. Figure **??** shows a histogram of the time of flight of all trigger photons. It shows a Gaussian shape centered around zero with a tail for $t < 0$ which comes from pile up events that are eliminated by the TOF cut.
7. **Charged Hadron Veto Cut:** Clusters were checked to see that they did not match with the angle of a track as measured by the PC3. This is an elliptical cut of 12 cm in z and 8 cm in ϕ. The matching track was required to have quality ≥ 7 and $p_T > 0.5$ GeV. This cut did not require that the area of the PC3 in front of the photon cluster be live and if no charged track was found the photon passed this cut.

In order to be included in the direct photon sample, photons needed to pass the following cuts:

1. **ERT Check:** The super module of the trigger photon was required to match with the super module that fired one of the ERT triggers.
2. **Tagging cut:** Used to reduce background from $\pi^0 \to \gamma\gamma$ and $\eta \to \gamma\gamma$ decays. More details in the next paragraph of this section.
3. **Isolation Cut:** requires that the photon have much more energy than everything surrounding it in the detector and is used to further suppress background from decay photons as well as NLO fragmentation photons. More details for this cut are listed later in this section.

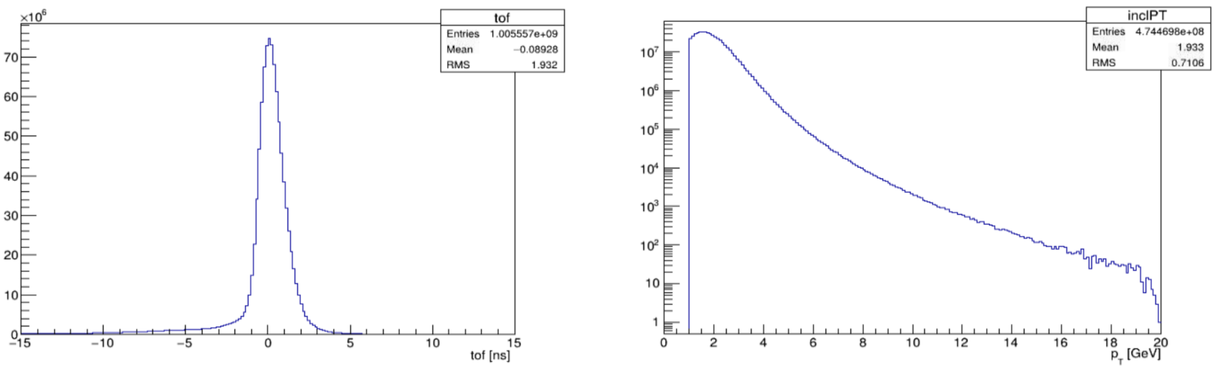

(a) Time of fight

(b) p_T

Figure 1: ERT trigger photon TOF and p_T distributions

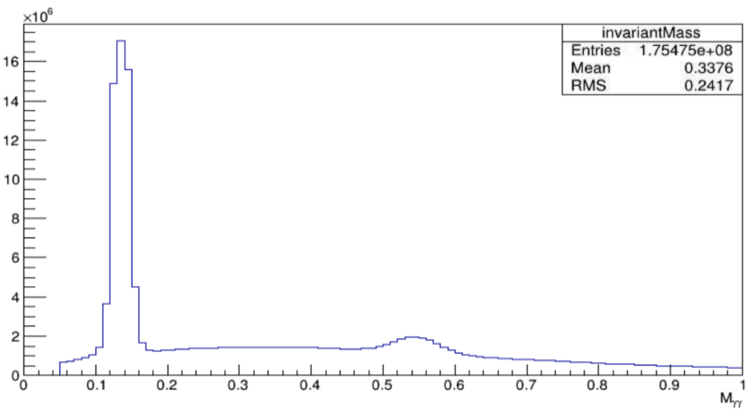

Figure 2: Invariant mass plot of all found photon pairs.

For the tagging cut, each photon cluster was cross checked with every other cluster in the event to see if together they made an invariant mass pair that could reconstruct to an $h \to \gamma\gamma$ decay. This second photon was first required to pass all of the general photons cuts listed before. The photons in this pairs then needed to be:

1. in the same arm
2. have the central tower of their clusters be more than 8 cm apart
3. have invariant mass of $0.105 < M_{\gamma\gamma} < 0.165$ GeV for π^0 tagging and $0.480 < M_{\gamma\gamma} < 0.620$ GeV for η tagging.

Figure 2 shows the invariant mass cuts for photon pairs that pass all but the very last pair cut. The raw numbers from this tagging cuts are listed in Table 1. All of the photons that contributed to these numbers were required to pass the the photon isolation cut from Equation 1 not the pair isolation cut from Equation 15, which will be explained more in the next paragraph.

There are much fewer $\eta \to \gamma\gamma$ photons than $\pi^0 \to \gamma\gamma$, and so photon pairs within the η invariant mass peak have a much high fraction contribution from combinatorial background. There was therefore initially some concern that a large portion of the direct photons could be getting mistakenly matched with a photon and form a pair that happened to have an invariant mass within the η range of $0.480 < M_{\gamma\gamma} < 0.620$ GeV. Table 1 shows that this is clearly not the case since so few photons get eliminated by the η tagging cut to being with.

In the isolation cut, a photon is required to have ten times the energy of all of the event activity surrounding it. E_{cone} is the sum of all of the energies of the surrounding clusters and the momenta of all of

p_T [GeV]	Isolated Direct Photon Candidates (Does Not Include Tagged Photons)	Isolated Photons Eliminated Because of π^0 Tagging	Isolated Photons Eliminated Because of η Tagging
5 to 6	817,509	10,335	2,561
6 to 8	339,584	11,959	2,707
8 to 10	60,164	3,014	715
10 to 18	25,371	1,278	307

Table 1: Isolated Photon counts from the tagging cuts

the surrounding tracks that are within $r = \sqrt{\Delta\phi^2 + \Delta\eta^2} < 0.4$ radians. It is used in the photon isolation cut formula:

$$E_\gamma * 10\% > E_{cone} \tag{1}$$

where E_γ is the energy of photon that may or may not pass this cut. All of the clusters that enter into this cone energy sum have to pass the following cuts:

1. $E > 0.15$ GeV
2. 3x3 cut of warn map and dead map clusters
3. Hot tower cut - Eliminates clusters whose central tower is either in or adjacent to a hot tower
4. $|TOF| < 5$ ns
5. Charged Hadron Veto Cut (same cut as described in the list of photon cuts above).

The charged hadron veto cut ensures that that any charged hadron that ideposits energy in the EMCal and is reconstructed as a charged track is not double counted in E_{cone}. No shower shape cut is used on these clusters, however, such that if a charged hadron deposited energy in the EMCal but was not reconstructed as a track, it could still be included in E_{cone}. For a track to be included into into this cone sum it needed:

1. mom > 0.2 GeV
2. quality > 7
3. pc3sdphi < 4 and pc3sdz < 4

Previous direct photon analyses also had a maximum momentum cut off for tracks, requiring mom < 15 GeV in order to avoid including tracks $\gamma \to e^+e^-$ conversion that were reconstructed with an incorrectly large momentum due to their lack of curvature. This cut was not used in this analysis's cone sum because it was agreed that even if the e^+e^- tracks were reconstructed with an artificially large momentum, they still represent event activity that should be taken into account when deciding whether or not a photon is isolated. There is also the slightly different photon *pair* isolation cut that is used to quantify the direct photon background, which will be described in detail in Section 5. The direct photon candidate p_T spectrum is shown in Figure 3. The average p_T value for each p_T bin is summarized in Table 2.

p_T[GeV]	Bin Center [GeV]
5 to 6	5.39
6 to 8	6.69
8 to 10	8.77
10 to 18	11.9

Table 2: Central Value for Each p_T bin

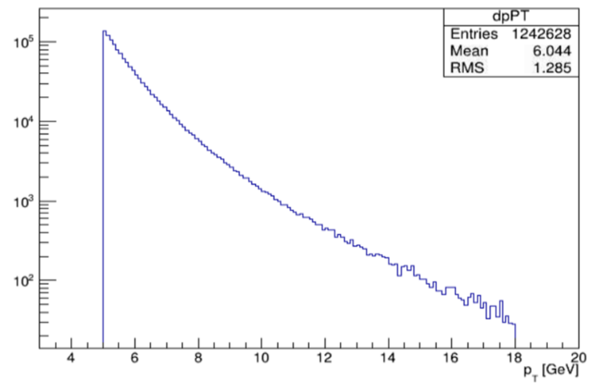

Figure 3: Direct Photon candidate p_T spectrum

3.3 Polarization

The proton beam is never 100% polarized collisions from unpolarized protons dilute the A_N measurement. This needs to be corrected by dividing by the average beam polarization. The fill by fill polarization values for each beam were taken from the official CNI polarimetry group values and are shown in Figure 4. Because of lack of statistics, this analysis combined data from two different fills when calculating the asymmetry. These fills we grouped together chronologically (i.e. the first two fills of Run15 became the first group, the third and fourth fills became the second group and so on) and the polarization of each fill group was the average polarization of the two fills weighted by the fill luminosity.

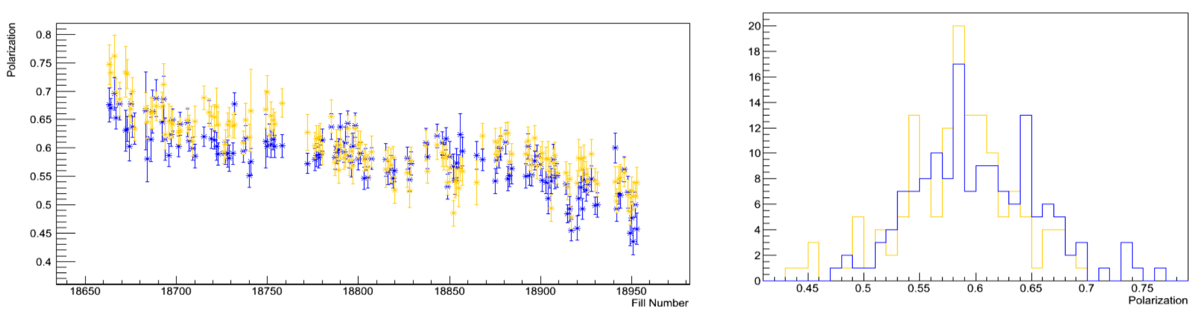

Figure 4: Fill by fill polarization

3.4 Relative Luminosity

The Relative Luminosity asymmetry formula uses counts that are only on one side of the detector at a time and then calculates the asymmetry for when the beam was spin up versus spin down. Any detector effects cancel out in the ratio, but the particle yields need to be corrected if there were more $p^{\uparrow} + p$ than $p^{\downarrow} + p$ or vice versa, also known as the relative luminosity. For transverse single spin asymmetries this quantity is defined as $R = L^{\uparrow}/L^{\downarrow}$.

The relative luminosity of each fill group was calculated by summing up the bunch by bunch GL1P BBCLL1 (BBC with 30 cm vertex cut) scalers taken from the spin data base for each run in that fill group. This was done separately for each beam, using the spin pattern for those fills, which was also taken from the spin database. The sum of the scalers for when the crossing was spin up was divided the sum of the scalers for when the crossing was spin down. It should be noted that for Run 15 a value of -1 corresponds that the beam was polarized up (towards the sky in the actual experiment) and value of +1 corresponds to the beam being polarized down (towards the ground). Figure 5 shows the relative luminosity calculated for per fill.

As stated in Section 3.1 the outlier fills 18777 and 18778 were eliminated from asymmetry calculations. The relative luminosities used in this analysis were calculated for each fill group of two.

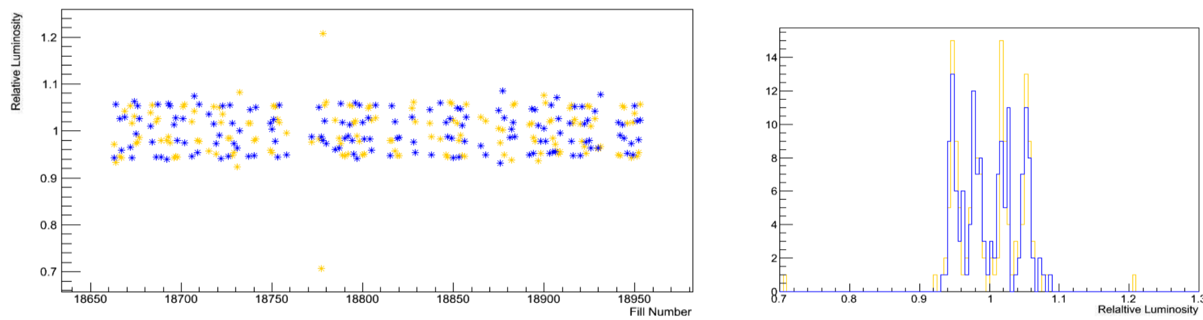

Figure 5: The relative luminosity calculated fill by fill

3.5 Azimuthal Correction

Traditionally, raw transverse single spin asymmetries $\epsilon_N(\phi)$ are measured as a function of ϕ and then fit to a sinusoid to extract the amplitude A_N and then corrected for the polarization P:

$$\epsilon_N(\phi) = A_N * P * \cos\phi \tag{2}$$

This formula follows the conventions that $\phi = 0$ is 90^0 to the left of the spin direction, making $\phi = 0$ and $\phi = \pi$ the places where the asymmetry is maximal. For this analysis this method is not practical since the asymmetry is consistent with zero, has limited statistics, and only 180^o of ϕ acceptance, so these asymmetries integrate over the ϕ range of each arm. Thus an azimuthal correction $\langle | \, cos\phi \, | \rangle$ is needed to correct for the dilution of this true physics asymmetry over this large range in ϕ. Assuming uniform azimuthal coverage across the PHENIX central detector would make the acceptance correction:

$$\langle | \, cos\phi \, | \rangle = \frac{\int | \, cos\phi \, | \, d\phi}{\int d\phi} = \frac{2}{\pi}\left(cos(\frac{3\pi}{16}) - cos(\frac{11\pi}{16}) \right) \approx 0.883 \tag{3}$$

But as Figure 6 clearly shows, the distribution of direct photon candidates is not quite flat in ϕ. Not only are there gaps between the sectors where edge tower cuts were performed, but there are also some fluctuations in yields across sectors where there are dead areas. The block on the left side of Figure 6a corresponds to the sector on the bottom of the west arm and the block on the right side of Figure 6b corresponds to the PbGl sector on the bottom of the east arm. Previous versions of this analysis note showed lead glass sectors having a much lower direct photon candidate yield when compared to the lead scintillator sectors, this is because at that time there was no hot tower cut on clusters going into cone sum for the isolation cut, which affect the PbGl sectors more since they have many more hot towers.

Because the ϕ distribution is not flat across both arms we must instead find the average $| \cos\phi \, |$ for each direct photon candidate, separately for each arm:

$$\langle | \, cos\phi \, | \rangle = \frac{\sum_{i=1}^{N} | \cos\phi_i \, |}{N} \tag{4}$$

The values used are summarized in Table 3, where the west and wast arm values are used for the Relative Luminosity Formula. The "both" quantity is used in the Square Root Formula and is the average of the west and east arm values, weighted by the total counts in each arm.

4 Results Before Background Correction

At RHIC the transverse polarization either points up to the sky or down to the ground, which can be used to construct transverse single spin asymmetry formulas where systematic effects like relative luminosity and

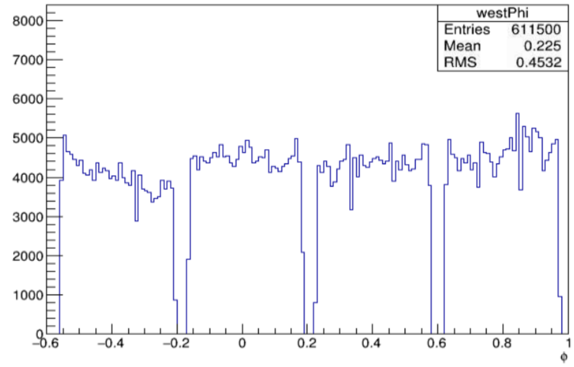

(a) West Arm

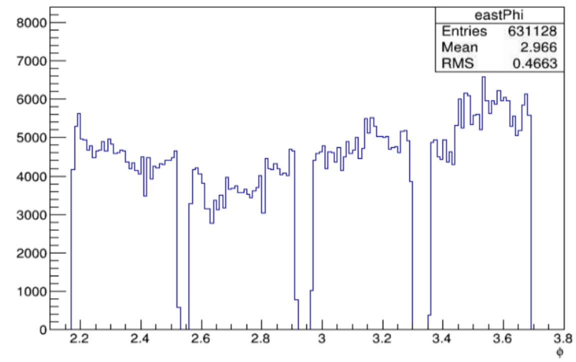

(b) East Arm

Figure 6: ϕ distribution for direct photon candidates with $5 < p_T < 18$ GeV

Arm	$\langle \mid cos\phi \mid \rangle$
West	0.878
East	0.882
Both	0.880

Table 3: Azimuthal correction using ϕ values from measured direct photon candidates

detector efficiency cancel out. The raw asymmetry is corrected by the dilution of the beam not being 100% polarized and for integrating over the azimuthal range of the detector:

$$A_N = \frac{1}{\langle \mid cos\phi \mid \rangle} \frac{1}{P} A_N^{raw} \tag{5}$$

$$\sigma_{A_N} = |A_N| \sqrt{\left(\frac{\sigma_{A_N^{raw}}}{A_N^{raw}}\right)^2 + \left(\frac{\sigma_P}{P}\right)^2} \tag{6}$$

Because there were not enough statistics to calculate the asymmetry separately for each fill, the corrected asymmetry was calculated for fills in groups of two as described in Section 3.3.

4.1 Square Root Formula

The Square Root Formula combines data from both arms and proton beam polarization configuration. It is not an exact expression for the asymmetry, but to first order effects from both detector acceptance and the relative luminosity cancel out. Equation 7 and 8 show the expression of the raw asymmetry where the up and down arrows indicate the beam polarization direction and the L and R subscripts indicate either to the left or the right of the polarized beam going direction (i.e. the east arm is to the left of the yellow beam going direction but to the right of the blue beam). Because the statistical uncertainty formula in Equation 8 assumes Poison statistics, each count category that was used in this calculation ($N_L^\uparrow$, $N_R^\uparrow$,$N_L^\downarrow$, or $N_R^\downarrow$) was required to have at least 10 counts for each fill group and p_T bin.

$$A_N^{raw} = \frac{\sqrt{N_L^\uparrow N_R^\downarrow} - \sqrt{N_L^\downarrow N_R^\uparrow}}{\sqrt{N_L^\uparrow N_R^\downarrow} + \sqrt{N_L^\downarrow N_R^\uparrow}} \tag{7}$$

$$\sigma_{A_N^{raw}} = \frac{\sqrt{N_L^\uparrow N_R^\downarrow N_L^\downarrow N_R^\uparrow}}{(\sqrt{N_L^\uparrow N_R^\downarrow} + \sqrt{N_L^\downarrow N_R^\uparrow})^2} \sqrt{\frac{1}{N_L^\uparrow} + \frac{1}{N_L^\downarrow} + \frac{1}{N_R^\uparrow} + \frac{1}{N_R^\downarrow}} \tag{8}$$

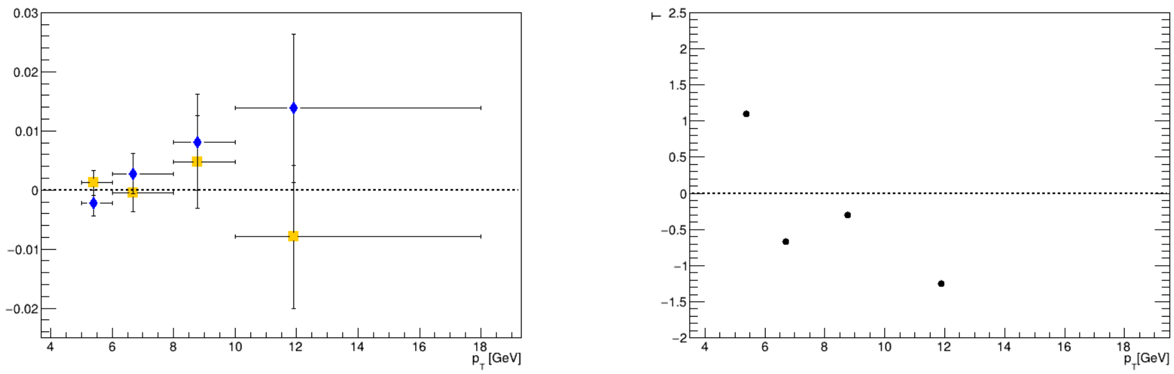

Figure 7: Before background correction blue and yellow beam square root formula results

Since both proton beams are polarized, there are two statistically independent measurements of the asymmetry when considering the polarization of the yellow beam and averaging over the polarization of the blue beam, or vice versa. Figure 7 shows the final yellow and blue beam asymmetry results and a T test which evaluates whether or not the difference between the beams is statistically significant:

$$T(p_T) = \frac{A_N^{Yellow} - A_N^{Blue}}{\sqrt{(\sigma^{Yellow})^2 + (\sigma^{Blue})^2}} \tag{9}$$

There is a plus sign in the denominator of this formula because the yellow and blue beam results are completely statistically independent. If the differences in the blue and yellow beam were not statistically significant, we would expect the T values to follow a Gaussian distribution with an even split between positive and negative values and approximately 60% of with a magnitude less than 1. While it is difficult to apply a Guassian distribution to four data points, Figure 7 shows that two out of four of the T values have a magnitude that is less than 1 and one T value is slightly larger than 1. And while three points being negative and one point being positive is not an even split, it is one point away from being an even split.

4.2 Relative Luminosity Formula

The Relative Luminosity Formula is an alternative way of calculating a Transverse Single Spin Asymmetry and an exact formula for for the asymmetry. Because it takes the ratio of counts that are all found in the same side of the detector, effects from acceptance and detector efficiency effects cancel out. So instead of being literally a left vs right asymmetry, this is a beam polarization up vs down asymmetry, which means it needs to be corrected for the relative luminosity $R = L^{\uparrow}/L^{\downarrow}$ (from Section 3.4) of the beam configurations.

$$A_N^{raw} = \frac{N_L^{\uparrow} - R \cdot N_L^{\downarrow}}{N_L^{\uparrow} + R \cdot N_L^{\downarrow}} \tag{10}$$

$$\sigma_{A_N^{raw}} = \frac{2RN_L^{\uparrow}N_L^{\downarrow}}{\left(N_L^{\uparrow} + R \cdot N_L^{\downarrow}\right)^2}\sqrt{\frac{1}{N_L^{\uparrow}} + \frac{1}{N_L^{\downarrow}}} \tag{11}$$

There is an equivalent formula for the right side counts, but the signs in the numerator are flipped to preserve the TSSAs left-right convention. This statistical error formula also assumes Poison Statistics and so it was again required that each count category used ($N_L^{\uparrow}$ and $N_L^{\downarrow}$ or $N_R^{\uparrow}$ and $N_R^{\downarrow}$) have 10 counts or more per each fill group and p_T bin. It was also assumed that the statistical error in relative luminosity values is negligible.

In addition to the statistically independent blue and yellow beam asymmetries, there are two asymmetries for each side of the detect, giving a total of four statically independent measurements to compare. Figure 8 shows the left and right formula results for the blue and yellow beams along with a T test evaluating the

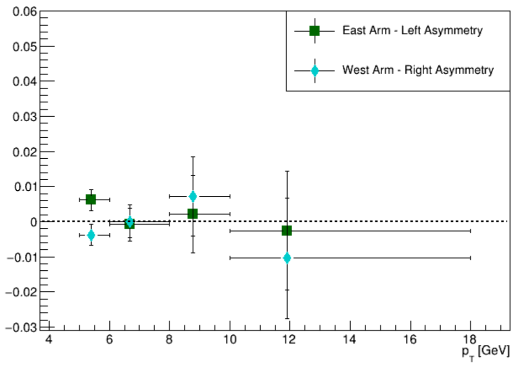

(a) Yellow beam

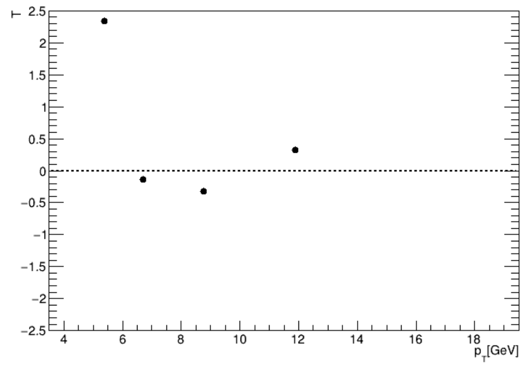

(b) T test of yellow beam left and right asymmetries

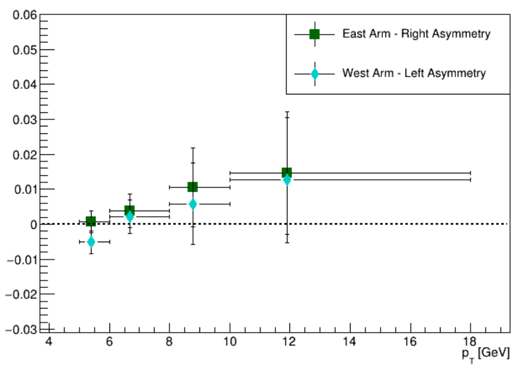

(c) Blue beam

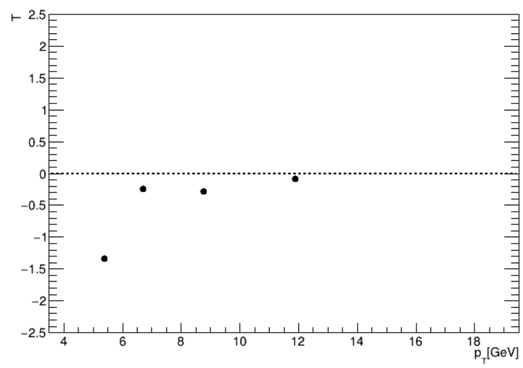

(d) T test of blue beam left and right asymmetries

Figure 8: Before background correction results for the relative luminosity formula asymmetry

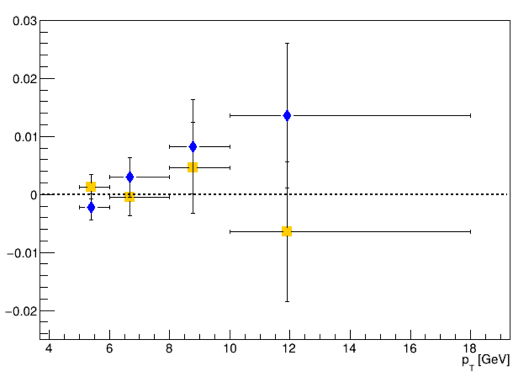

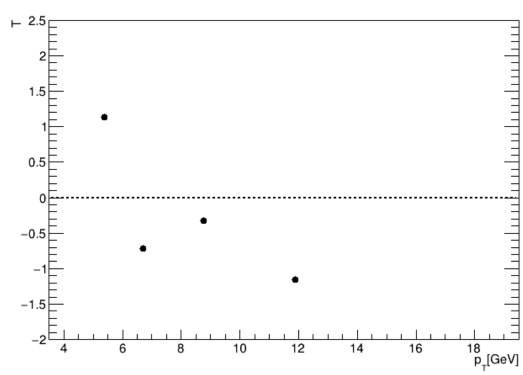

Figure 9: Before background correction blue and yellow beam relative luminosity formula results

statistical significance of the differences in left and right asymmetries:

$$T(p_T) = \frac{A_N^{Left} - A_N^{Right}}{\sqrt{(\sigma^{Left})^2 + (\sigma^{Right})^2}} \tag{12}$$

Six out of eight of the T values in Figure 8 have a magnitude that is less than 1 and three out eight of them are either positive or very slightly negative. The plots in Figure 9 are the weighted average of left and right asymmetries from Figure 8 for the respective beam polarization. The plots look very similar to the plots in Figure 7, which is expected given that they are measuring the asymmetry with the exact same data set.

4.3 Comparing Results From Different Formulas

The Relative Luminosity Formula and Square Root Formula results calculate the asymmetry slightly differently but with the exact same data set and so they are 100% correlated. Thus the T test formula used to evaluate the statistical significance of the differences between the formulas has a minus sign in the denominator:

$$T(p_T) = \frac{A_N^{Sqrt} - A_N^{Lumi}}{\sqrt{|(\sigma^{Sqrt})^2 - (\sigma^{Lumi})^2|}} \tag{13}$$

Figure 10 shows the results for comparing the Square Root and Relative Luminosity Formulas. The asymmetries in Figures 10a and 10c and the exact same results as were shown in Figures 7 and 9, just plotted in a different combination. The asymmetries in Figure 10e are the weighted average of the blue and yellow beam asymmetry for the respective formula. The T values in this figure might be slightly larger and tend to be more negative than one would expect if they were to show that the differences between the two formulas are statistically consistent, but these asymmetries have not yet been corrected for background. All asymmetries shown in Figure 10 are consistent with zero across p_T.

4.4 $A_N \sin\phi$ Modulation Cross Check

Even though it is not practical for this analysis to measure the asymmetry as a function ϕ, it still serves a good way to check the integrating over ϕ methods from before and as a way of verifying that the azimuthal correction was done correctly. The $\sin\phi$ modulation was done using the Relative Luminosity Formula, because the ϕ dependent Square Root Formula requires every piece of the detector have another part of the detector 180 degrees away for it.The PHENIX arms are not back to back, but slightly offset, so using the Square Root Formula would mean throwing out all of the data from top sector of each arm. The Relative Luminosity Formula focuses on one portion of the detector at a time and takes advantage of the fact that the spin direction can flip on a bunch by bunch:

$$A_N * sin(\phi_s) = \frac{1}{P}\epsilon_N(\phi_s) = \frac{1}{P}\frac{N^{\uparrow}(\phi_s) - R \cdot N^{\downarrow}(\phi_s)}{N^{\uparrow}(\phi_s) + R \cdot N^{\downarrow}(\phi_s)} \tag{14}$$

where the angle ϕ_s is zero at the spin up direction (y = 0 in PHENIX coordinates) and increases to the left of the polarized beam going direction to maintain that A_N is a left-right asymmetry. One asymmetry was calculated per each fill group, p_T bin, and ϕ bin. Each count that was used in the asymmetry ($N^{\uparrow}, N^{\downarrow}, N^{\uparrow}$, and $N^{\downarrow}$) was still required to be at least 10. P are the polarization polarization values that were found in Section 3.3 and the R are the same relative luminosity values from Section 3.4. No azimuthal correction was needed because we are no longer integrating over ϕ. Then the asymmetries for each p_T and ϕ bin were then averaged over all fill groups.

Each arm was split into thirds in ϕ because it is the minimum amount of points needed to constrain a sine function. Figure 11 shows these averages asymmetries as a function of ϕ_s and fit to this function: "[0]*sin(x)". The central ϕ value that was used in all of these fits was the average ϕ value for all photons in that p_T and ϕ bin. Almost all of the χ^2/dof values are less than 1 indicating that error bars are too large to constrain the sinusoid. Fingure 12a shows these fit values plotted at a function of p_T for both the yellow and blue arm. As expected, the plot looks very similar to the blue and yellow asymmetries for both the Relative Luminosity and Square Root asymmetries from earlier sections. Figure 12b shows the weighted average of the fit values for the blue and yellow beam in purple and in red is the averaged blue and yellow asmmetries

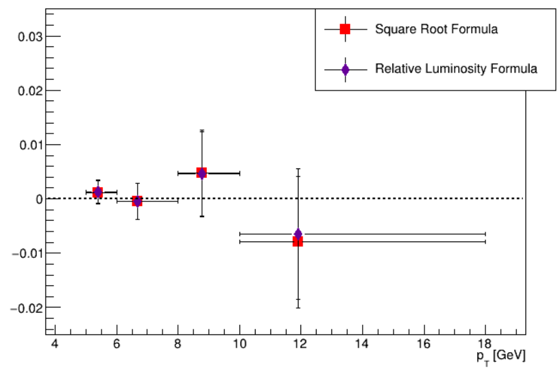

(a) Yellow beam

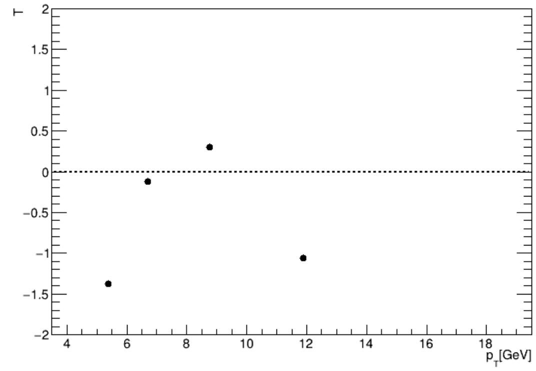

(b) T test of yellow beam asymmetries

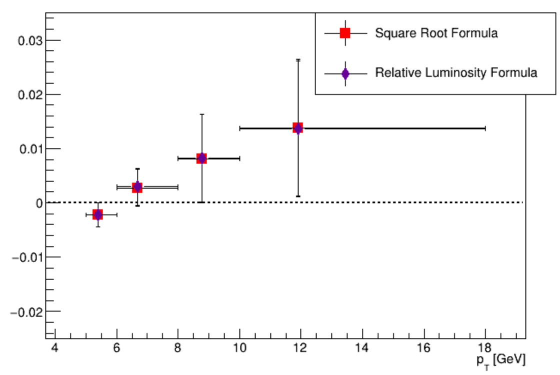

(c) Blue beam

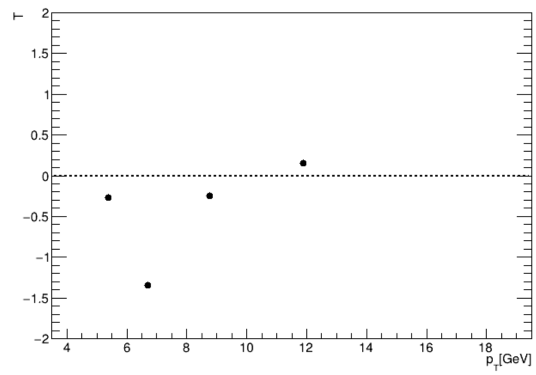

(d) T test of blue beam asymmetries

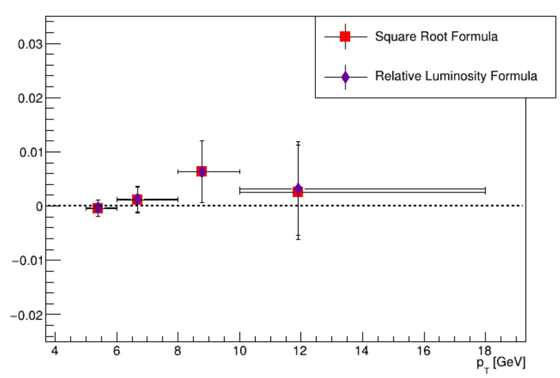

(e) Final asymmetries

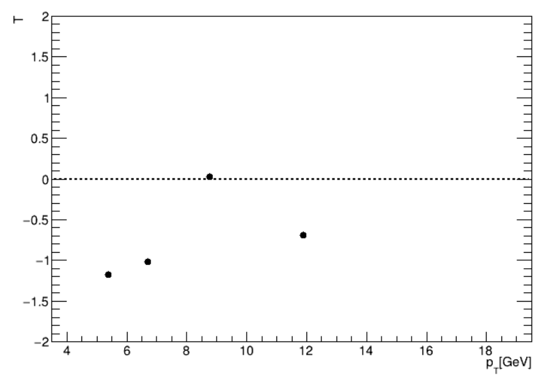

(f) T test of final asymmetries

Figure 10: Comparing formulas results before the asymmetry was corrected for background

from the Relative Luminosity Formula from Figure 9. These results are in very good agreement, with the worst agreement at the highest p_T bin where low statistics meant that a lot more counts got thrown out to meet the “at least 10” requirement, especially since these counts were being split into three separate ϕ bins. The fact that these two methods are in such good agreement indicates not only that the asymmetry is in general being calculated correctly, but that the azimuthal correction is also correct.

5 Background Correction

The main source of background for isolated direct photons is photons that came from a hadronic decays that are not eliminated by the tagging cut. For an $h \to \gamma\gamma$ there are three interesting things that can happen: (1) both photons are measured, (2) only one of the photons is measured, and (3) the two photons are so close together that they are reconstructed as a single photon, also known as merging. When both photons are measured, these photons are eliminated from the direct photon sample by the tagging cut. The main source of background for direct photons (especially at PHENIX) is (2) when the second photon is missed either because it was out of acceptance, it hit a dead area of the detector, or it's energy was too low to pass the minimum energy requirement of 0.5 GeV. Photon merging is a smaller effect and will be discussed in Section 5.3. This section will use the the following notation for the different types of photon counts:

- N^{iso} - The direct photon sample, isolated photons where the photons that were tagged as coming from either π^0 or η decays have already been eliminated
- N^{iso}_{tag} - Photons that were tagged as coming from either a $\pi^0 \to \gamma\gamma$ or $\eta \to \gamma\gamma$ decay that are in an isolated photon pair. This is not a subset of N^{iso}.
- N^{iso}_{miss} - Isolated photons that came from hadronic decays, but the second photon was missed and they were not eliminated by the tagging cut. This is a subset of N^{iso} and must be estimated using Monte Carlo.
- N^{iso}_{merge} - Merged $\pi^0 \to \gamma\gamma$ clusters that pass the photon isolation cut. These are part of the background of N^{iso} and need to be estimated using Monte Carlo.

Photon pairs are selected using the same requirements for the tagging cut that was explained in Section 3.2. For a photon with energy E_γ that has been matched into a pair with a second photon of energy E_{pair}, in order for this first photon to pass the *pair* isolation cut it must have:

$$E_\gamma * 10\% > E_{cone} - E_{pair} \tag{15}$$

This pair isolation cut is slightly more lenient than the photon isolation cut from Equation 1 with the idea being that if the energy from second photon E_{pair} had been missed than this photon with energy E_γ would have passed the photon isolation cut and been added to the direct photon sample. Figure 13 shows the p_T distributions for photons from isolated pairs that were tagged as coming from either $\pi^0 \to \gamma\gamma$ ($0.105 < M_{\gamma\gamma} < 0.165$ GeV) or $\eta \to \gamma\gamma$ ($0.480 < M_{\gamma\gamma} < 0.620$ GeV) decays.

Since N^{iso}_{miss} is the main source of background for this analysis and a subset of N^{iso} the background fraction for this analysis is $r_{miss} = N^{iso}_{miss}/N^{iso}$. But since N^{iso}_{miss} cannot be measured directly in data, it is estimated using one miss ratio R from $h \to \gamma\gamma$ single particle Monte Carlo, which is explained in detail in Sections 7 and 8 of AN979 and Section 8 of AN460. R is the ratio of the number of photons where only pone of the decay photons was measured divided by the number of photons where both photons were measured: $R = N_{miss}/N_{tag}$. It can then be used to convert N_{tag} to N_{miss} making the expression for the background fraction become: $r_{miss} = N^{iso}_{miss}/N^{iso} \approx R \times N^{iso}_{tag}/N^{iso}$. The makes the background subtraction formula for this analysis:

$$A_N^{dir} = \frac{A_N^{iso} - r_{\pi^0} A_N^{iso,\pi^0} - r_\eta A_N^{iso,\eta}}{1 - r_{\pi^0} - r_\eta} \tag{16}$$

where $r_{\pi^0} = R_{\pi^0} \frac{N^{iso,\pi^0}_{tag}}{N^{iso}_{tag}}$ and $r_\eta = R_\eta \frac{N^{iso,\eta}_{tag}}{N^{iso}_{tag}}$. Both the background fraction and background asymmetries need to be measured a function of photon p_T to avoid having to do the complicated conversion between hadron and decay photon p_T.

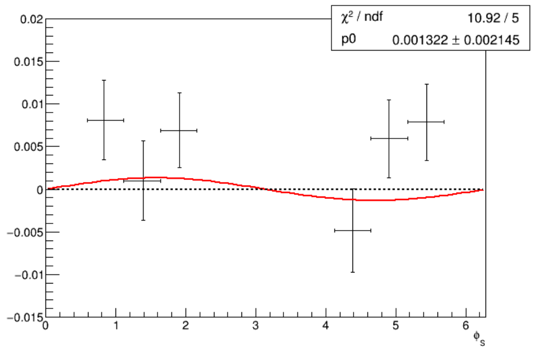

(a) Yellow Beam $5 < p_T < 6$ GeV

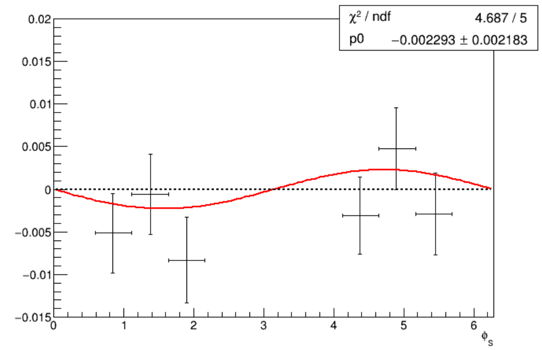

(b) Blue Beam $5 < p_T < 6$ GeV

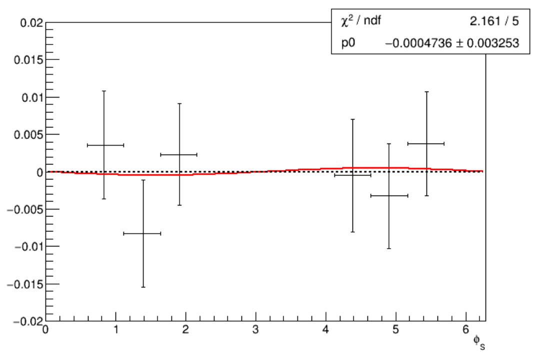

(c) Yellow Beam $6 < p_T < 8$ GeV

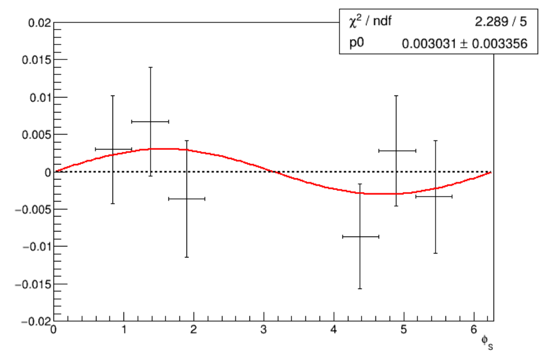

(d) Blue Beam $6 < p_T < 8$ GeV

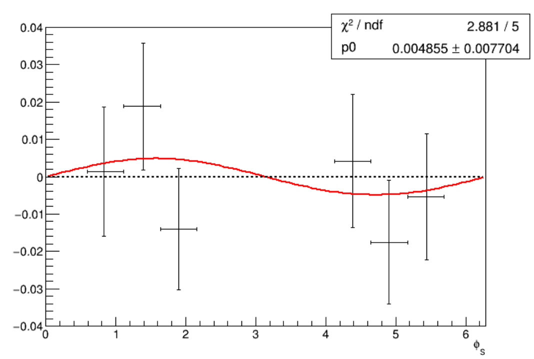

(e) Yellow Beam $8 < p_T < 10$ GeV

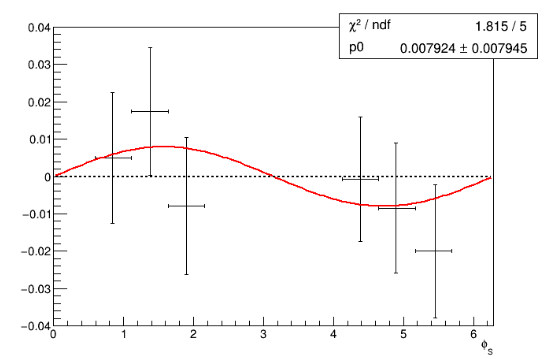

(f) Blue Beam $8 < p_T < 10$ GeV

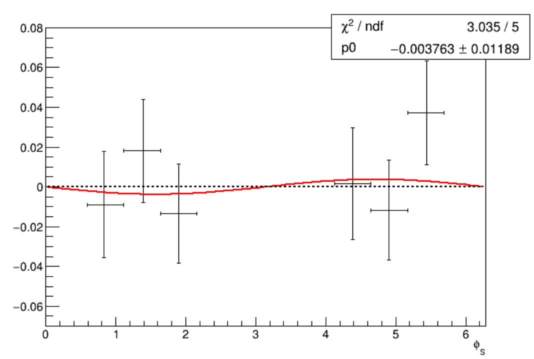

(g) Yellow Beam $10 < p_T < 18$ GeV

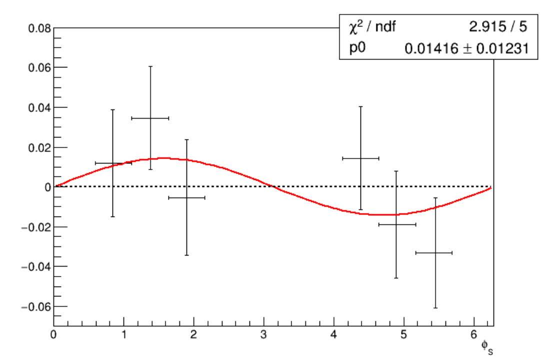

(h) Blue Beam $10 < p_T < 18$ GeV

Figure 11: A_N $\sin\phi$ Modulation Fits

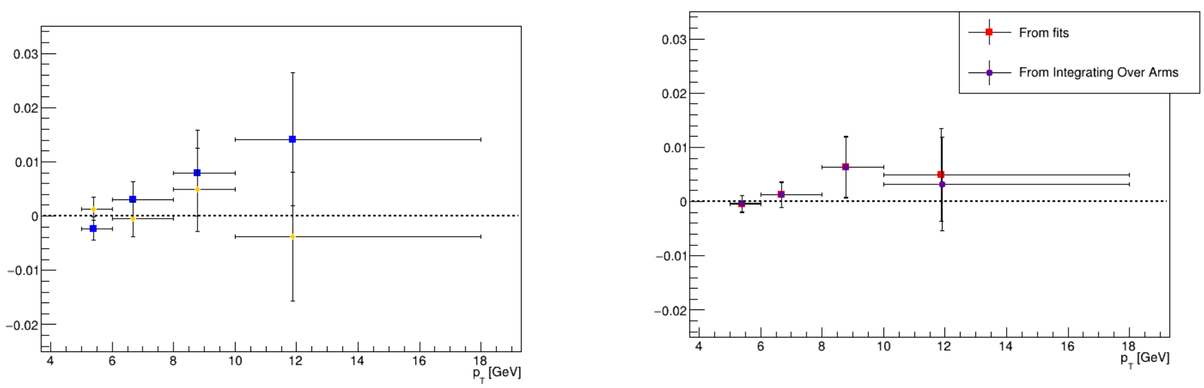

(a) Blue and yellow beam results from fits

(b) Comparing methods for the final Relative Luminosity Formula result

Figure 12: Asymmetry results from fitting A_N $\sin(\phi_s)$

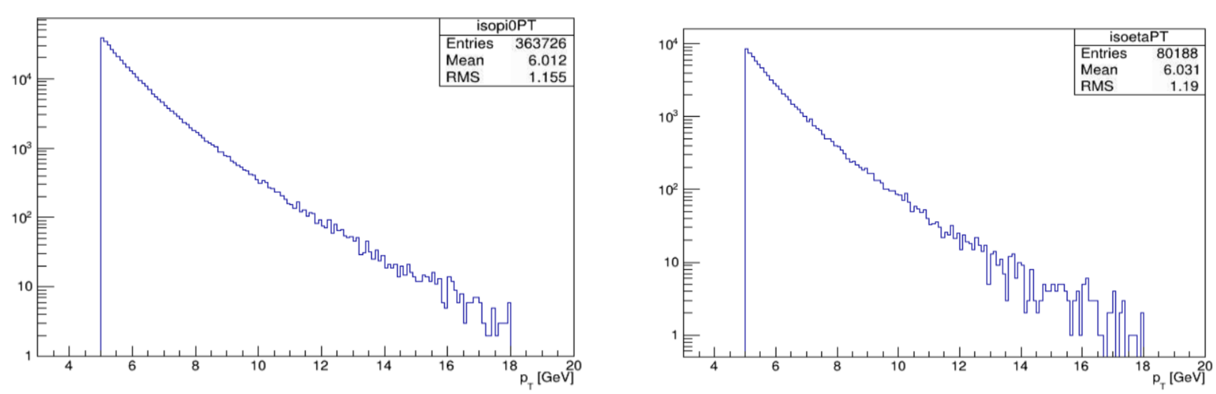

(a) N_{tag}^{iso,π^0}

(b) $N_{tag}^{iso,\eta}$

Figure 13: Isolated tagged photon pair distributions as a function of photon p_T

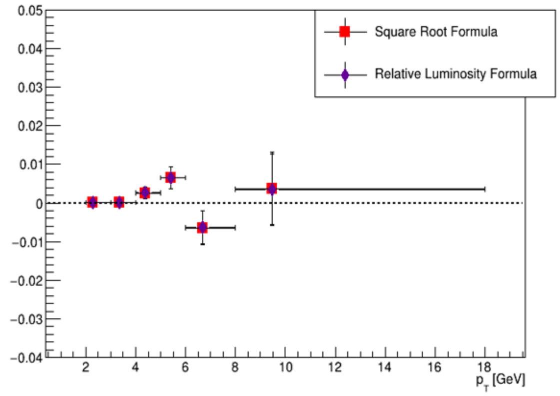

(a) $A_N^{iso,\pi^0}(p_T^\gamma)$

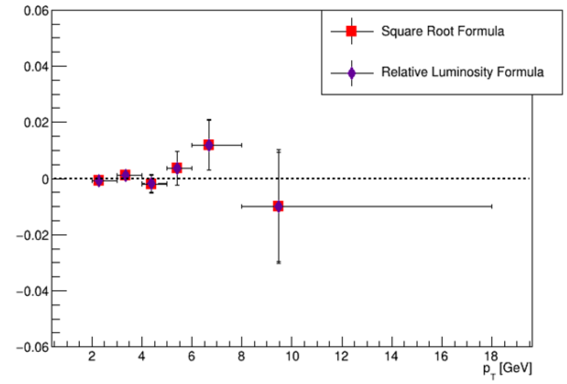

(b) $A_N^{iso,\eta}(p_T^\gamma)$

Figure 14: Direct Photon Background Asymmetries

5.1 Background Asymmetries

The background asymmetries in Equation 16 are consistent with zero statistically limited partially because of the pair isolation cut, but mostly because they are calculated as a function of photon p_T. Figure 14 shows the beam averaged asymmetries for isolated π^0 and η photons in a slightly wider photon p_T range than what is being used for this analysis. These were calculated using fill groups of 3 and with a azimuthal correction calculated for each set of photons from isolated pairs using the same method as described in Section 3.5. Each count category was still required to have 10 or more photons, which meant the last two p_T bins in the analysis had to be combined.

Instead of plugging in the background asymmetries into Equation 16 and blowing up the statistical uncertainty of the direct photon result, the background asymmetries are instead set to zero. This treats the background essentially as a dilution: there is some direct photon physical asymmetry that is being diluted by photons from π^0 and η decays whose A_N is zero and thus the direct photon asymmetry must be rescaled by one minus the background fraction:

$$A_N^{dir} = \frac{A_N^{iso}}{1 - r_{\pi^0} - r_\eta} \tag{17}$$

5.2 Background Fraction

As has already been discussed, the background fraction calculation for this analysis has two parts: $N_{tag}^{iso,h}/N_{tag}^{iso}$ which is calculated in from data and the one miss ratio R_h which is calculated from single particle Monte Carlo. Figure 15 shows the $N_{tag}^{iso,h}/N_{tag}^{iso}$ ratios as a function of photon p_T, using much finer binning than what is used for this asymmetry analysis. These ratios are simply the photon p_T distributions seen in Figure 13 divided by the the p_T distribution for direct photon candidates from in Figure 3. The ratios in Figure 15a are larger than the ratios in Figure 15b because there are simply less η photons than π^0 decay photons. This is partially because there are just less η mesons produced and partially because the $\pi^0 \to \gamma\gamma$ branching ratio is about 99% while the $\eta \to \gamma\gamma$ ratio is about 40%. The shape in the distribution is controlled by the distance between the two decay photons: at low p_T less photon pairs are measured because the decays are more asymmetric so it is more likely that one of the photons is missed and at high p_T less photon pairs are measured because the decays are more symmetric and so the photons are more likely to merge. The ratios are slightly larger in the west arm for the both of the hadrons, especially at low p_T, this is because the east arm has comparatively more dead area and the denominator only requires measuring one photon, while the numerator requires measuring two. The ratios in the west and east arm get closer in value with increasing p_T because the PbGl sectors in the east arm have a higher spacial resolution than the PbSc sectors. Table 4 shows the final values for these ratios of yields in the p_T bins of this analysis.

The next part of the background fraction is the one miss ratio R which is calculated from single particle

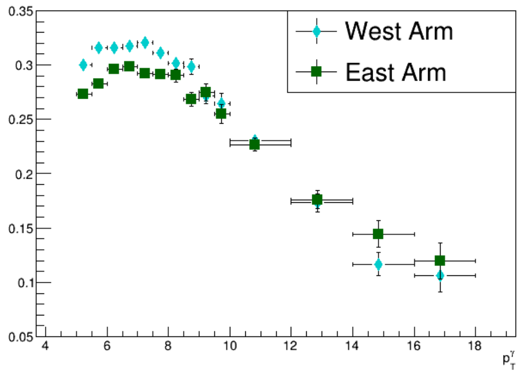

(a) $N_{tag}^{iso,\pi^0}(p_T^\gamma)/N_{tag}^{iso}(p_T^\gamma)$

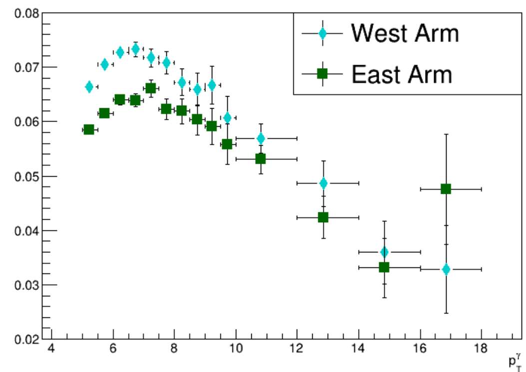

(b) $N_{tag}^{iso,\eta}(p_T^\gamma)/N_{tag}^{iso}(p_T^\gamma)$

Figure 15: Ratio of isolated tagged photon pairs divided by direct photon candidates

	$N_{tag}^{iso,\pi^0}/N_{tag}^{iso}$		$N_{tag}^{iso,\eta}/N_{tag}^{iso}$	
p_T [GeV]	West Arm	East Arm	West Arm	East Arm
5 to 6	0.305 ± 0.00010	0.276 ± 0.00092	0.068 ± 0.00042	0.059 ± 0.00039
6 to 8	0.317 ± 0.0016	0.296 ± 0.0015	0.072 ± 0.00068	0.064 ± 0.00063
8 to 10	0.290 ± 0.0036	0.276 ± 0.0034	0.066 ± 0.0015	0.060 ± 0.0014
10 to 18	0.202 ± 0.0044	0.204 ± 0.0044	0.052 ± 0.0021	0.049 ± 0.0020

Table 4: Isolated tagged photon pairs divided by direct photon candidates

Monte Carlo. 20 million π^0 and η mesons were generated separately by exodus. They used a power law for the p_T spectrum using -8.122 for the exponent for π^0 and -8.192 for η, which come from fits to previous PHENIX cross sections that are explained in the next paragraph. For the rest of the kinematics: $| z_{vtx} | \leq 30$ cm was to match the rest of the analysis, $4 < p_T < 30$ GeV was used avoid any edge effects from the p_T range and $-0.5 < y < 0.5$ and $0 < \phi < 2\pi$ to be able to fully measure the effect of one of the photons missing the detector. These particles were then run through PISA, converted into a DST, and run through a modified version of the `offline/AnalysisTrain/Run15ppPhotons` taxi code, making sure to only process $h \to \gamma\gamma$ decays.

The exponent for the power law came from fits to previous cross sections measurements for $p_T > 5$ GeV. The fits are shown in Figure 16, where the π^0 cross section came from PPG063 and the η cross section from PPG107. The fit function that was used was "[0]*pow(x, [1])" and Figures 16c and 16d provide a quantitative way of evaluating it by plotting the difference in the cross section and fit values, normalized by the cross section's statistical error. Since all of the points are within about 2σ and the measured cross section is not systematically higher or lower than the fit, these fits are at lease reasonable enough to make kinematics of the simulations more realistic when compared to a flat p_T distribution.

The reconstruction efficiencies in Figure 17 serve as a cross check of the single particle Monte Carlos and plot the number of mesons that were reconstructed as diphoton pairs, divided by the number of truth mesons that had ϕ within the region of each arm, as a function of meson p_T. As expected, the reconstruction efficiency is higher in the west arm because there is less dead area and there are less η mesons reconstructed compared to π^0s due to the lower branching fraction. The shape of the efficiency distributions are consistent with what is expected: at lower p_T the reconstruction efficiency is suppressed by asymmetric decays causing the detector to miss at least one of the photons until about 12 GeV where the merging effects starts to turn on. The efficiency fall of due to merging is less steep in the east arm due to the higher granularity of the PbGl sectors. In Figure 17b the effects of from merging are not seen because η mesons do not start to merge until much higher p_Ts that this analysis.

Figure 18 shows the comparison of $1 + R$ for π^0 decays from this result compared to Figure 2 from PPG136 as a function of photon p_T, where $R = N_{miss}/N_{tag}$. Only clusters that had contributions from

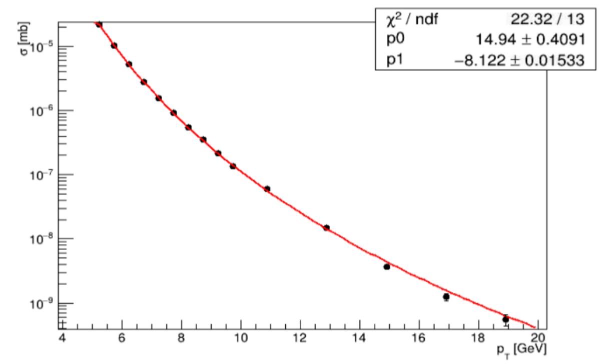

(a) π^0 cross section from PPG063

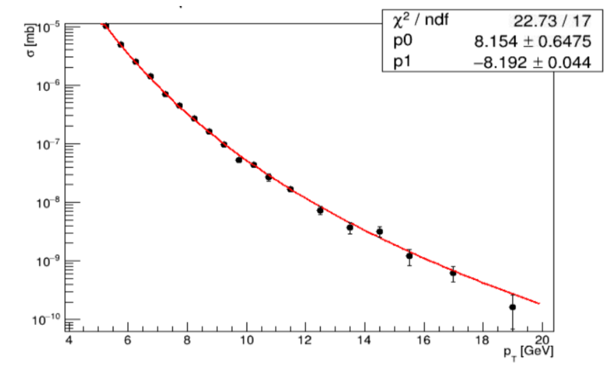

(b) η cross section from PPG107

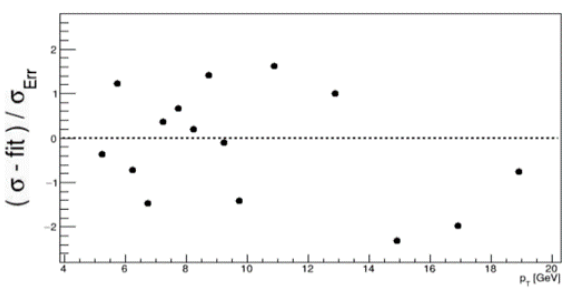

(c) Difference between the measured π^0 cross section and the fit, divided by the cross section's statistical error

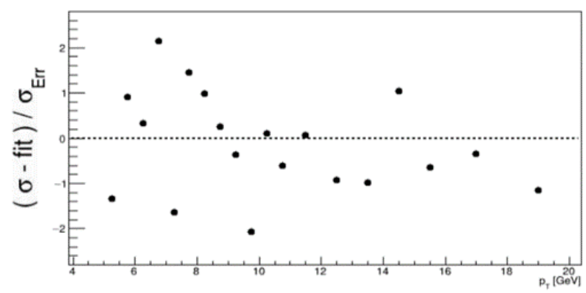

(d) Difference between the measured η cross section and the fit, divided by the cross section's statistical error

Figure 16: Power law fit to previously published PHENIX cross sections

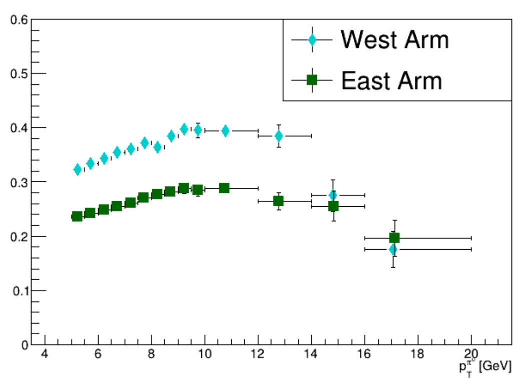

(a) π^0 Single Particle Monte Carlo

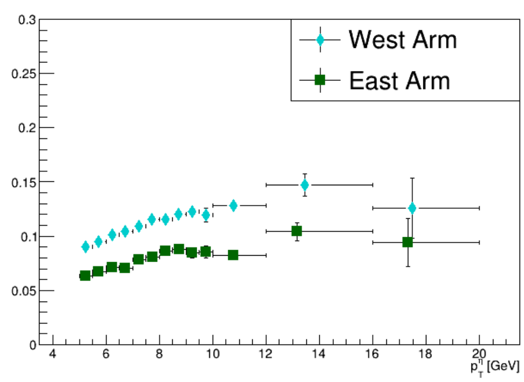

(b) η Single Particle Monte Carlo

Figure 17: Reconstruction Efficiency from Single Particle Monte Carlo

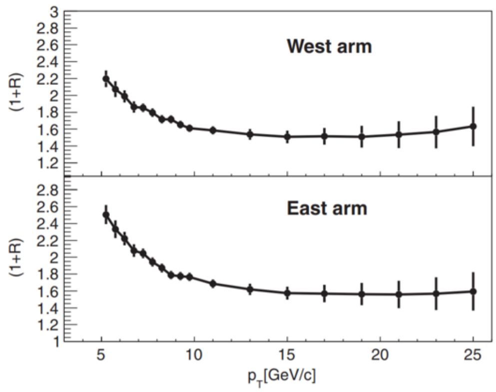

(a) Fig 2 of PPG136

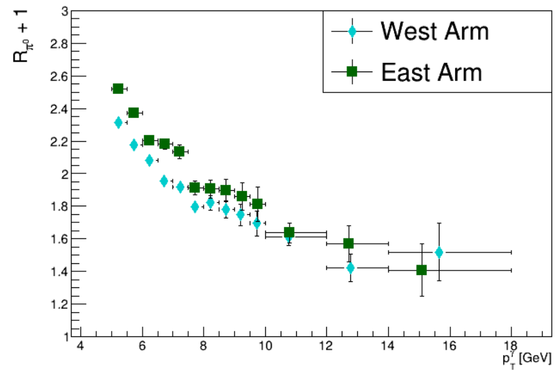

(b) This analysis's result

Figure 18: Comparing the π^0 one miss ratio to previous measurements

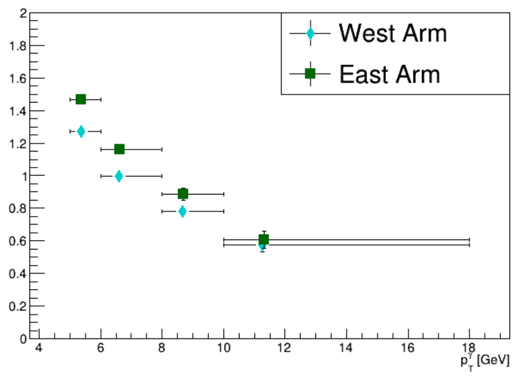

(a) π^0

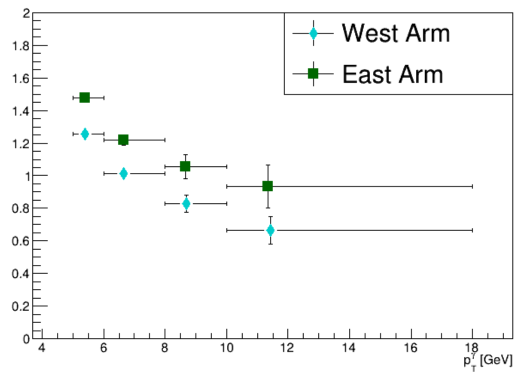

(b) η

Figure 19: One miss ratio for hadron diphoton decays using the p_T bins for the analysis

a single decay photon could contribute to the numerator and the denominator could include either photon from a $h \to \gamma\gamma$ decay (provided it had high enough p_T). The one miss ratio is used to convert the number of hadronic diphoton decays into the numbers that were missed. For example, since the $1 + R$ is 2.2 in the west arm for photon $p_T^\gamma = 5$ GeV, if 100 photons of $p_T^\gamma = 5$ GeV were tagged as coming from $\pi^0 \to \gamma\gamma$ decays in the west arm, then there were in reality 220 photons and 120 of them were missed. The values from these plots are fairly consistent by not exact given that the PPG136 plots used EMCal efficiencies from Run06 and this result used PISA settings for Run15. Across p_T the $1 + R$ values are larger in the east arm which is consistent with the east arm having more dead area and thus missing more photons. Figure 19 and Table 5 show the final R values for both π^0 and η decays. Again the all of the one miss values are larger in the east arm because more photons are missed due to the greater amount of dead area. R_η is also consistently slightly larger than R_{π^0} because η diphoton decays tend to be more asymmetric than π^0 decays because they have four times that mass and therefore access to more phase space.

Table 6 shows the final background fraction values from missing the second photon in π^0 and η diphoton decays where $r_h = R_h \frac{N_{tag}^{iso,h}}{N^{iso}}$. Across p_T bins the background fractions range from 12% to 40% for π^0s and 4% to 9% for ηs. As expected the background fractions are consistently larger in the east arm. The uncertainties on r are calculated using standard error propagation from the statistical error. These uncertainties are used in Section 7 to find a systematic uncertainty due to the uncertainty on r. Note the uncertainty on r_{π^0} for the highest p_T will increase once it takes into account π^0 merging, which is described in the next section.

	R_{π^0}		R_η	
p_T [GeV]	West Arm	East Arm	West Arm	East Arm
5 to 6	1.258 ± 0.009	1.476 ± 0.012	1.255 ± 0.017	1.480 ± 0.023
6 to 8	1.008 ± 0.012	1.159 ± 0.016	1.013 ± 0.022	1.220 ± 0.031
8 to 10	0.776 ± 0.028	0.933 ± 0.038	0.830 ± 0.052	1.054 ± 0.073
10 to 18	0.616 ± 0.047	0.673 ± 0.060	0.665 ± 0.084	0.934 ± 0.131

Table 5: One miss ratio for π^0 and η decays

	r_{π^0}		r_η	
p_T [GeV]	West Arm	East Arm	West Arm	East Arm
5 to 6	0.384 ± 0.003	0.409 ± 0.004	0.085 ± 0.001	0.087 ± 0.001
6 to 8	0.320 ± 0.004	0.343 ± 0.005	0.073 ± 0.002	0.078 ± 0.002
8 to 10	0.225 ± 0.009	0.257 ± 0.011	0.055 ± 0.004	0.063 ± 0.005
10 to 18	0.124 ± 0.010	0.137 ± 0.012	0.035 ± 0.005	0.046 ± 0.007

Table 6: Final background fraction due to missing the second photon in π^0 and η diphoton decays

5.3 Photon Merging

When a hadron decays into two photons in its rest frame, the photons will travel back to back. In the lab frame, where the decaying hadron was boosted, the photons travel with some decay angle between them. The faster the hadron was traveling, the smaller the decay angle tends to be. Eventually these photons get so close together that due to the finite spacial resolution of the EMCal, they can can no longer be distinguished as two separate photon clusters and instead one high p_T merged photon cluster is reconstructed. Because of the smaller tower size, $\pi^0 \to \gamma\gamma$ merging effect turns on at higher π^0 p_T in PbGl sectors when compared to PbSc, as can be clearly seen in the π^0 separation efficiency plotted Figure 20.

Photon merging was studied using single particle Monte Carlo. 10 million of the 20 million $4 < p_T < 30$ GeV π^0s produced in Section 5.2 were used to calculated the quantities in Figures 20a and 22 for p_T below 8 GeV. In order to have enough statistics at higher p_Ts an additional 1 million π^0 were produced with the same simulation parameters but with $8 < p_T < 30$ GeV. These simulated hadrons were used to calculate quantities in Figures 20a and 22 for p_T above 8 GeV. These particles were then run through PISA and then PISAtoDST and then a modified version of Run15ppPhotons taxi code. It was first required that only two photons from a π^0 decay hit the EMCal in order to avoid effects from conversion, missing acceptance, and so on. Then it was required that both of these photons hit an active part of the EMCal, so not on the edge of the sector and not near any dead or warn towers. Once a energy cut of $E > 0.5$ GeV was applied, if there were two clusters measured then this was considered a tagged π^0 and if there was only one cluster

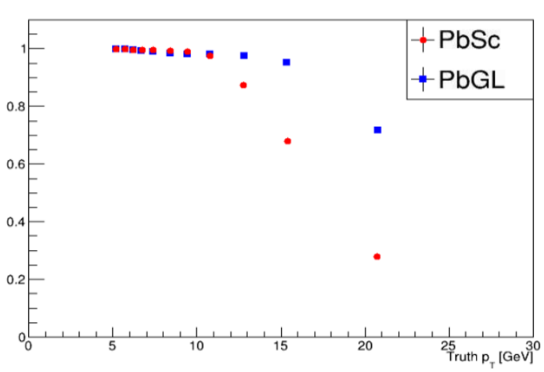

(a) Separation efficiency produced for this analysis

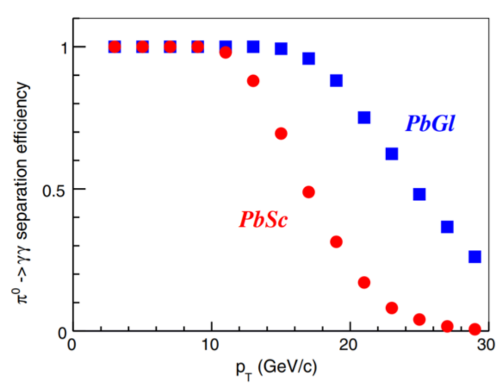

(b) Figure 1 from PPG186

Figure 20: $\pi^0 \to \gamma\gamma$ Separation Efficiency

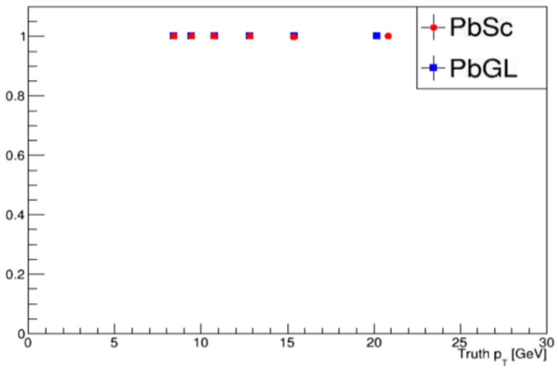

Figure 21: $\eta \to \gamma\gamma$ Separation Efficiency is 100%

than this cluster was considered merged. Additionally to better reproduce previous results, both particle tracks that contributed to a merged cluster were required to have efrac (energy deposited by particle track in EMCal associated with this cluster, divided by total energy measured in this cluster before shower shape corrections) to be greater than 0.005. The resulting separation efficiency as a function of truth π^0 p_T is shown in Figure 20a. To compare to previous π^0 cross section results, the clusters included in the plot have not yet been required to pass a shower shape cut which will eliminate the majority of merged clusters. Figure 20b shows the separation efficiency from Figure 1 of PP6186 where a fast Monte Carlo simulation was used. The slight differences in efficiency values comes from PPG186 using an energy asymmetry cut of $\alpha = |E_1 - E_2|/(E_1 + E_2) > 0.8$ instead of a minimum energy $E > 0.5$ GeV in order to increase the π^0 reconstruction efficiency.

Because η mesons are about four times as heavy than π^0s, $\eta \to \gamma\gamma$ decays merge at momenta higher than the scope of this measurement. To verify that the procedure for finding merged clusters was correct, this study was repeated for 1 million $8 < p_T < 30$ ηs generated by single particle Monte Carlo, using the same parameters and power law p_T spectrum as described in Section 5.2. Figure 21 shows the 100% separation efficiency that was found for ηs.

To find the uncertainty on the background fraction from merged π^0s a similar method to calculating the background fraction r_{miss} was used. N^{iso}_{merged} is the number of background isolated merged clusters. It cannot be measured directly in data, but with simulation we can learn how to convert between the number of clusters that have been tagged as coming from π^0s to the number of merged as a function of cluster p_T. So the background fraction becomes:

$$r_{merge} = \frac{N^{iso}_{merge}}{N^{iso}} \approx \frac{N_{merge}}{N_{tag}} \frac{N^{iso,\pi^0}_{tag}}{N^{iso}} \tag{18}$$

The $N^{iso,\pi^0}_{tag}/N^{iso}$ are the same values in Table 4 that were calculated from data and used for the previous background fraction calculation. The N_{merge}/N_{tag} values are calculated using this single particle Monte Carlo study and are shown in Figure 22. These plots are as a function of reconstructed cluster p_T, so either photon in tagged π^0 photon pair can contribute to N_{tag} assuming it had high enough p_T. Figure 22a shows this conversion ratio before a shower shape cut was applied, and Figure 22b shows the ratio after all clusters were required to have prob photon> 0.02. As this plot clearly shows, the shower shape cut is doing its job and eliminating the vast majority of merged clusters. Since this is the shower shape cut that is used in the rest of the analysis, this cut will be used for the r_{merge} calculation.

Table 7 shows the final values for the background fraction due to π^0 merging. Asexpected, the values are much larger in highest p_T bin when compared to the lower ones, but still very small over all. N_{merge}/N_{tag} is slightly higher in the east arm compared to the west not because there are more merged clusters in the east arm, but because there is more dead area and so N_{tag} is smaller. Because r_{merge} is almost an order or magnitude smaller than the uncertainty on r_{π^0} from Table 6, r_{merge} will just be added to this uncertainty and contribute to the systematic uncertainty for the direct photon TSSA, as described in Section 7.

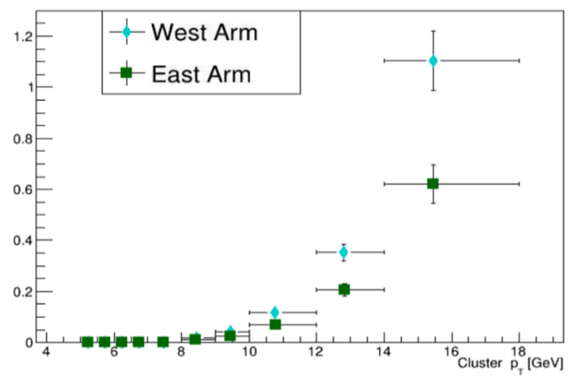

(a) N_{merge}/N_{tag} without a shower shape cut

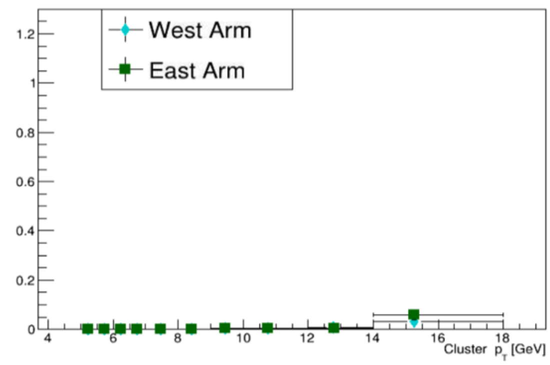

(b) N_{merge}/N_{tag} with a shower shape cut

Figure 22: N_{merge}/N_{tag} from single particle Monte Carlo

	West Arm			East Arm		
p_T [GeV]	$\frac{N_{merge}}{N_{tag}}$	$\frac{N^{iso}_{tag}}{N^{iso}}$	r_{merge}	$\frac{N_{merge}}{N_{tag}}$	$\frac{N^{iso}_{tag}}{N^{iso}}$	r_{merge}
5 to 6	0.0007	0.305	0.0002	0.0005	0.277	0.0001
6 to 8	0.0003	0.317	0.0001	0.0006	0.296	0.0002
8 to 10	0.0022	0.290	0.0006	0.0020	0.276	0.0005
10 to 18	0.0059	0.202	0.0012	0.0079	0.203	0.0016

Table 7: Background fraction due to π^0 merging. $r_{merge} = \frac{N_{merge}}{N_{tag}} \frac{N^{iso}_{tag}}{N^{iso}}$

5.4 Results After the Background Correction

Figure 23 shows the background corrected direct photon asymmetries after they have been rescaled by Equation 17. This equation is applied separately to all four the Relative Luminosity asymmetry results in Figure 8 and the blue and yellow beam Square Root Formula results from Figure 10d. The background fractions used for the square root formula correction are the average values for the east and west arm weighted by the total number of N^{iso} photons in each p_T bin. The T values are calculated using Equation 13 and are shifted slightly from the T values in Figure 10 now that the asymmetries have been corrected for background. Because they have only been rescaled by the background fractions, all asymmetries continue to be consistent with zero.

6 Systematic Cross Checks

6.1 Bunch Shuffling

Bunch shuffling is a technique used in RHIC asymmetry analyses to quantify the systematic uncertainty present in the data. It involves randomizing the polarization direction of the beam for each fill, bunch by bunch and recalculating the asymmetry using the same method as was used in calculate the physics asymmetry. In order to get enough shuffled asymmetries to properly study the variations in the data, this is done 10,000 times. Because the spin direction of the beam is now random, the physical asymmetry has been eliminated and any variation in asymmetry values beyond statistical fluctuation is due to systematic errors present in the data. Figure 24 shows the results of this study where each asymmetry value as a function of p_T was divided by the statistical error for that p_T bin and added to these histograms. Each one of these asymmetries was calculated using the Square Root Formula described in Section 4.1 to avoid having to recalculate the relative luminosity for each time all of the fills were shuffled. Just like the physics asymmetry, each shuffled asymmetry was calculated separately for each fill group of two and then averaged. As before each count category was required to be 10 or more such that the statistical error could be calculated using

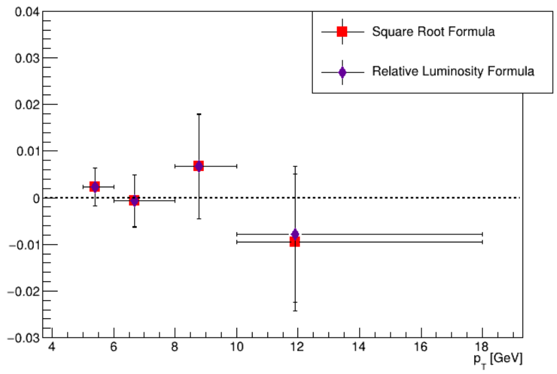

(a) Yellow beam

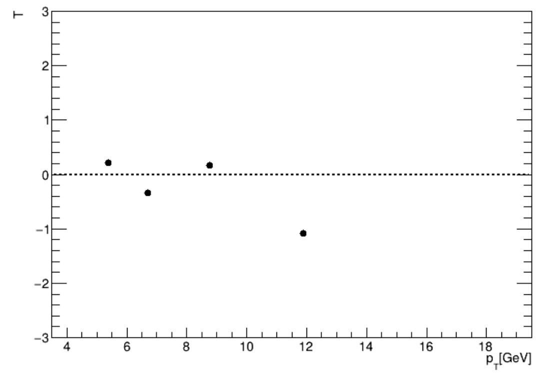

(b) T test of yellow beam asymmetries

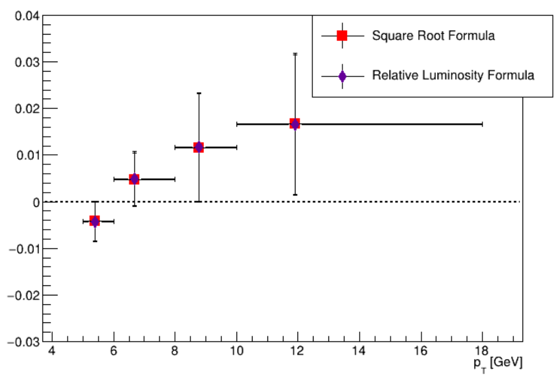

(c) Blue beam

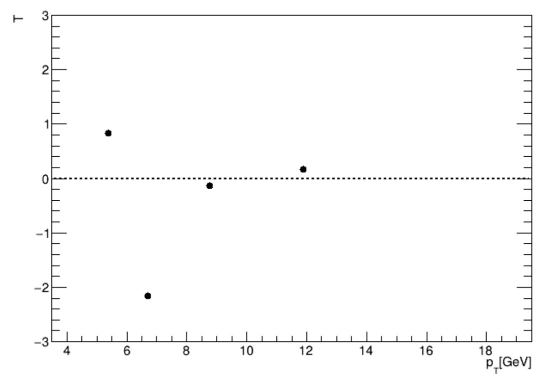

(d) T test of blue beam asymmetries

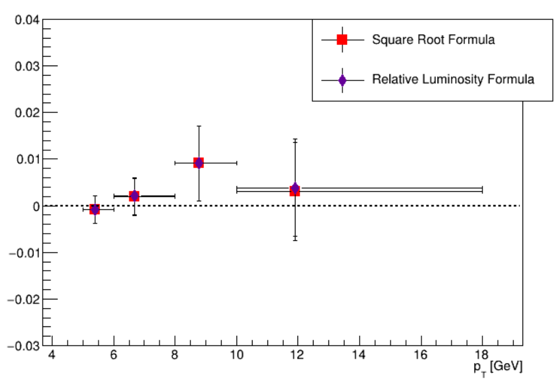

(e) Final asymmetries

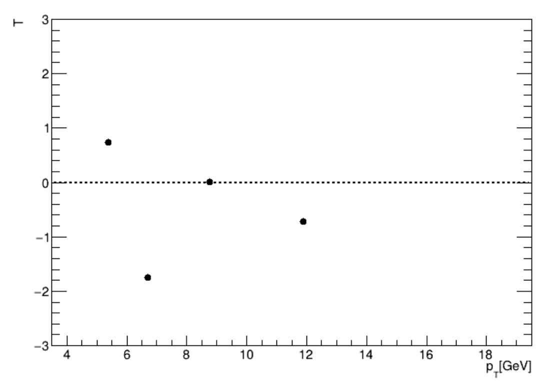

(f) T test of final asymmetries

Figure 23: Comparing asymmetry results from different formulas after the background correction

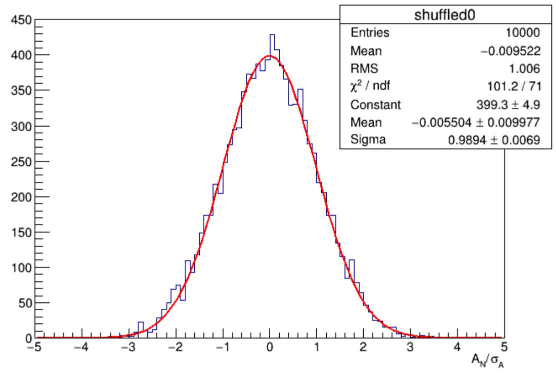

(a) $5 < p_T < 6$ GeV

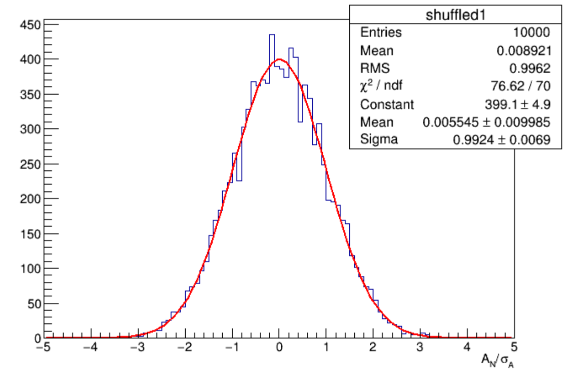

(b) $6 < p_T < 8$ GeV

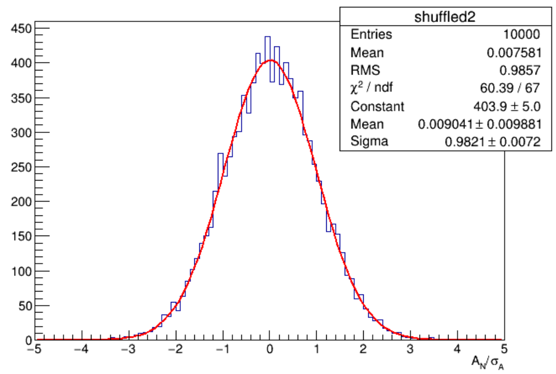

(c) $8 < p_T < 10$ GeV

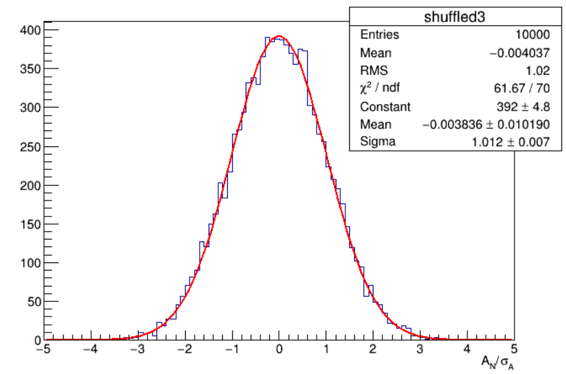

(d) $10 < p_T < 18$ GeV

Figure 24: Results from Bunch Shuffling

Poisson statistics. These distributions were then fit to a Gaussian to measure how closely they resembled random noise. As expected the mean of all of the fits is consistent with zero and the widths of these Gaussians are all very close to one.

6.2 Direct Photon Cross Section Cross Check

In order to verify that the direct photon yields of this analysis we consistent with previous results, the direct photon cross section was measured and compared to PPG136, PHENIX's previously published $\sqrt{s} = 200$ GeV direct photon cross section. To keep the calculation as simple as possible only ERT4x4a data was used because it was the only 4x4 ERT trigger that was taken in coincidence with the MB trigger with an online 30 cm vertex cut. Also only runs where the ERT4x4a scale down was set to zero were used, about 80% of runs. The cross section formula used for this calculation was:

$$E\frac{d^3\sigma_{dir}}{dp^3} = \frac{1}{\mathcal{L}} \cdot \frac{1}{2\pi} \cdot \frac{1}{p_T} \cdot \frac{1}{\epsilon^{trig}(p_T)} \cdot C^{geo}_{eff}(p_T) \cdot C^{BBCbias}_{p+p} \cdot \frac{N_{dir}}{\Delta p_T \Delta y} \tag{19}$$

Δp_T is the width of the p_T bin in units of GeV and Δy is set to 1 such that the cross section is calculated in 1 unit of rapidity. (PHENIX's limited psudeorapidity will be accounted for in the geometric efficiency factor $C^{geo}_{eff}(p_T)$). p_T is average p_T value for that bin listed in Table 2. $C^{BBCbias}_{p+p} = 1.337$ is the BBC trigger bias: even though the BBC efficiency is about 50% for all inelastic $p+p$ collisions, because of how PHENIX is optimized the BBC is has an efficiency of about about 75% for central ERT trigger events, the reciprocal of which is 1.337.

The integrated luminosity, $\mathcal{L}$, was found to be 36.62 pb^{-1}. The total number of events in the ERT sample that fired the ERT4x4a trigger and passed to offline 30 cm vertex cut was $7.64 \cdot 10^8$. This total number of

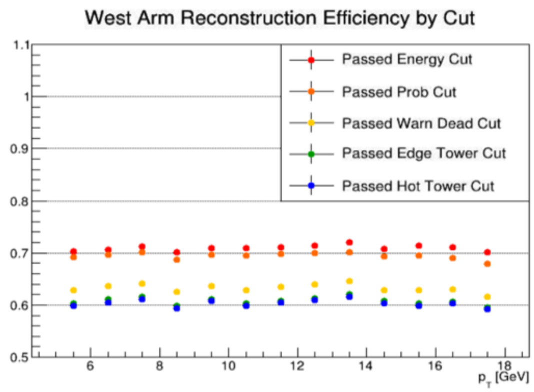

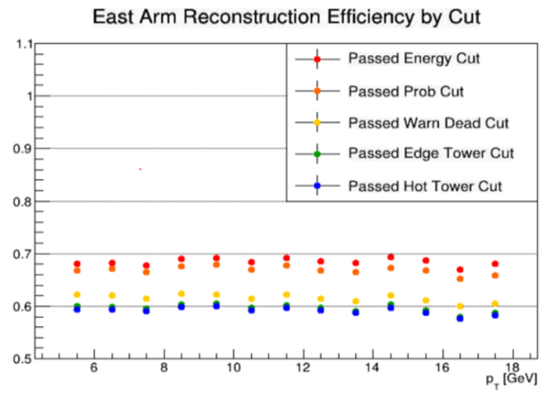

Figure 25: Cumulative cut by cut photon reconstruction efficiency

p_T [GeV]	$C^{geo}_{eff}(p_T)$
5 to 6	4.80
6 to 8	4.78
8 to 10	4.78
10 to 18	4.82

Table 8: Geometric efficiency factor for the cross section cross check

events is then divided by the BBC cross section $\sigma_{BBC} = 23$ mb, which takes into account the efficiency of the BBC. This quantity then had to be multiplied by the rejection factor: the number of events that fired the the BBCLL1 scaled trigger in the minimum bias sample divided by the number of events in this minimum bias sample that fired both the scaled BBCLL1 trigger and the live ERT4x4a trigger, which was found to be

$$\frac{N^{event}_{BBCLL1}}{N^{\gamma}_{ERT4x4a\&BBCLL1}} = \frac{1.59 \cdot 10^8}{1.44 \cdot 10^5} = 1103.3 \tag{20}$$

Both of these event counts also only included events that passed the offline 30 cm vertex cut. The rejection factor is necessary because the integrated luminosity is to be supposed calculated using the total number of $p+p$ collisions that were view, not the total that were recorded. Since the ERT trigger is about 1000 times more selective than minimum trigger, only using the total number of recorded ERT4x4a trigger events severely underestimates the integrated luminosity. This number does not represent the full integrated luminosity for Run15 $p+p$ collisions, but the integrated luminosity for ERT4x4a data in runs where the ERT4x4a scale down was set to zero.

The geometric efficiency factor, $C^{geo}_{eff}(p_T)$, corrects for the EMCal's limited acceptance, both from detector geometry and from data cuts. The geometric efficiency factor is approximately the reciprocal of the photon reconstruction efficiency multiplied by 2 for the central EMCal's limited ϕ acceptance and divided by 0.7 for the EMCal's limits η acceptance. The cumulative cut by cut reconstruction efficiency can be seen in Figure 25. (Cumulative meaning that reconstructed photons that contributed to the yellow "Passed Warn Dead Cut" points also passed the energy cut and the prob photon shower cut.) This was calculated using single particle Monte Carlo of 1 million photons that were generated by exodus with $|z_{vtx}| < 30$ cm and a flat p_T distribution with $4 < p_T < 30$ GeV. A wide angular range with $0 < \phi < 2\pi$ and $-0.5 < y < 0.5$ was used to capture the effects from the limited PHENIX geometric acceptance. These truth photons were then run through PISA, converted into a DST, and then run through a modified version of the Run15ppPhotons taxi code. In addition to passing all the cuts listed in the plot (which are the same as the cuts that were described in Section 3.2) the reconstructed photons were also required to have the majority of their energy coming from the original truth photon. The TOF cut was not used for the reconstruction efficiency or geometric efficiency factor calculations because it is expected to have an efficiency of about 100% and was found to be not well calibrated in this PISA simulation. The reconstruction effiency was calculated as the number of reconstructed photons divided by the number of truth photons within ϕ and η ranges of the respective arms

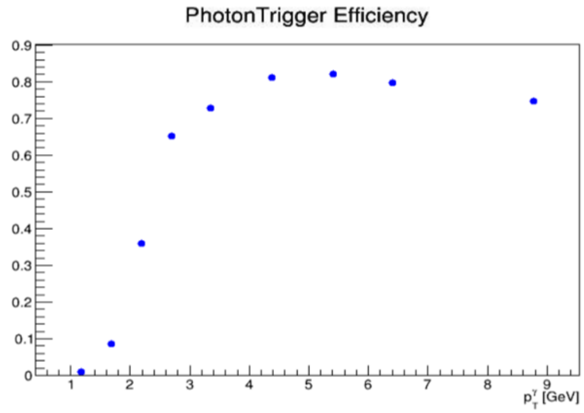

Figure 26: ERT Trigger Efficiency

p_T [GeV]	$N^{\gamma}_{ERT4x4a\&BBCLL1}$	N^{γ}_{BBCLL1}	ϵ^{trig}
5 to 6	284	346	0.82
6 to 8	127	159	0.80
8 to 18	29	42	0.69

Table 9: ERT Trigger Efficiency for the cross section cross check

as a function of truth p_T. There are very few photon that are eliminated by the hot tower cut because for cluster energies above 5 GeV there are only a total of 36 hot towers. The geometric efficiency factor was calculated as the ratio of the total number of simulated photons in that p_T bin divided by the total number of reconstructed photons as a function of truth p_T . These values are listed in Table 8.

$\epsilon^{trig}(p_T)$ is the ERT4x4a trigger efficiency. This was calculated using inclusive photon yields from the minimum bias sample. These inclusive photons passed all fiducial cluster cuts, but were not required to pass a tagging cut or isolation cut. The trigger efficiency is equal to ratio of the number of photons that fired both the scaled ERT4x4a and BBCLL1 triggers to the number the fired only the scaled BBCLL1 triggers:

$$\epsilon^{trig} = \frac{N^{\gamma}_{ERT4x4a\&BBCLL1}}{N^{\gamma}_{BBCLL1}} \tag{21}$$

Figure 26 shows the trigger efficiency for a wider p_T range than used in this analysis, showing the expected turn on shape that flattens out around $p_T = 5$ GeV. As Table 9 shows, there are not a large amount of inclusive photons with $p_T > 5$ GeV. So the trigger efficiency that was calculated using this method comes with a large statistical uncertainty, but for the purposes of a cross section cross check these values are satisfactory.

The direct photon yield N_{dir} is calculated using the following formula:

$$N_{dir} = N_{incl} - (1 + R_{\pi^0}) \cdot N_{\pi^0} - (1 + R_{\eta}) \cdot N_{\eta} \tag{22}$$

where N_{incl} is the number of inclusive photons without tagging cuts or an isolation cut and N_{π^0} and N_{η} are the number of photons that were tagged as coming from $\pi^0 \rightarrow \gamma\gamma$ and $\eta \rightarrow \gamma\gamma$ decays respectively. All three of these photon counts, N_{incl}, N_{π^0} , and N_{η} were required to be in a run where the ERT4x4a scaled down was set to zero, in an event that fired the scaled ERT4x4a trigger, and also in an EMCal supermodule that fired the ERT4x4a trigger. R_{π^0} and R_{η} are the one-miss ratios from Table 5 and allow us to estimate the number of background photons from missing the second photon in a $h \rightarrow \gamma\gamma$ by using the number of photons that were tagged as coming from a diphoton decay. Since the background behaves slightly differently in the west versus the east arms (as can be seen by the different one-miss ratios in Figure 19) the calculation was done separately for the west and east arms and then averaged together weighted by the statistical error. There was no isolation cut applied to this direct photon yield because because PPG136 did not use an isolation cut in their cross section calculation. The final direct photon yields can be seen in the second column of Table 10

p_T [GeV]	N_{dir}	This Result $E\frac{d^3\sigma}{dp^3}$ [pb/GeV^2]	PPG136 Average $E\frac{d^3\sigma}{dp^3}$ [pb/GeV^2]	Percent Difference
5 to 6	1.88e+05	1181.87	908.11	23.2%
6 to 8	8.52e+04	221.21	208.06	5.9%
8 to 10	1.71e+04	39.20	37.82	3.5%
10 to 18	8.48e+03	3.61	3.74	3.6%

Table 10: Comparing the cross section calculated for this result to PPG136

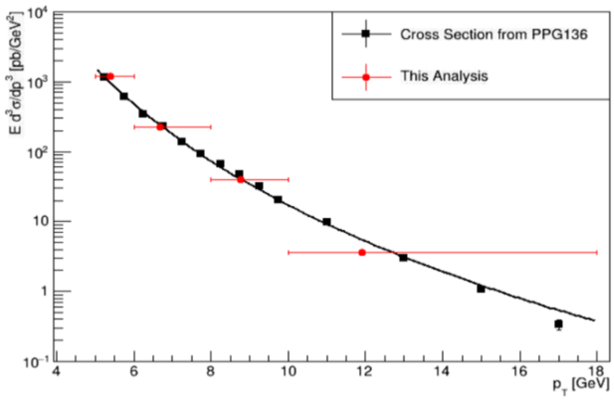

Figure 27: Cross Check comparing the inclusive direct photon cross section to PPG136

Figure 27 shows the final cross section for this analysis plotted with the PHENIX $\sqrt{s} = 200$ GeV cross section published in Table II of PPG136. These final cross section values are also listed in Table 10 and compared to the values from PPG136 averaged across this analysis's wider p_T bins. These averages were computed by fitting a power law to the published cross section, integrating across this analysis's wider p_T bins and then dividing by the width of that bin. The last column of Table 10 shows that this cross section cross check is on average with in 10% of the previously published results.

The direct photon asymmetry uses isolated direct photon yields, not inclusive so the isolated to inclusive ratios were compared to those from PPG136. This is not quite an apples to apples comparison because the isolation cut that was used for the published ratios was slightly different. Most notably, the radius used for the isolation cone in PPG136 was 0.5 radians instead of 0.4 and track momenta that was included in isolation cone was required to have $0.2 < p_{track} < 15$ GeV while this analysis only required $p_{track} > 0.2$ GeV. A detailed description of isolation cut of PPG136 can found on page 7 of PPG136 or Section 8 of AN979. The number of isolated direct photons is calculated using a slightly different formula:

$$N_{dir}^{iso} = N^{iso} - R_{\pi^0} \cdot N_{tag}^{iso,\pi^0} - R_{\eta} \cdot N_{tag}^{iso,\eta} \tag{23}$$

that uses the notation detailed at the beginning of Section 5. N^{iso} is the direct photon sample so the photons that were tagged as coming from π^0 and η decays have already been eliminated. Figure 28 shows the ratios of the isolated yields to inclusive yield for direct photons and photons that were tagged as coming from π^0 and η decays. The decay photons were required to pass the photon *pair* isolation cut, instead of the photon isolation cut. Though the magnitude of the direct photon and π^0 decay photons varies slightly between Figure 28a and Figure 28b, they show the same trends as a function of p_T.

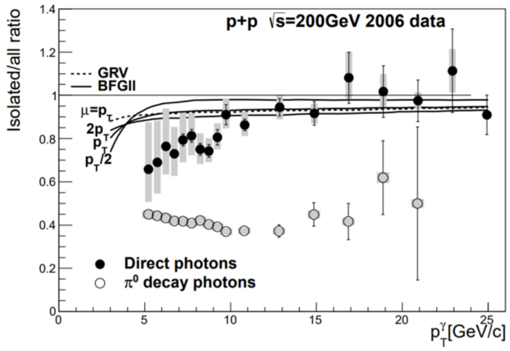

(a) Figured 13 of PPG136

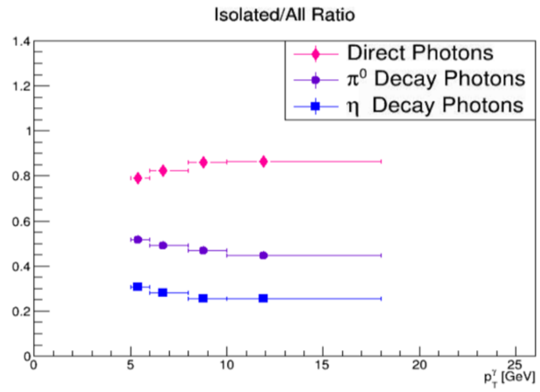

(b) Isolated over inclusive photon yields

Figure 28: Comparing isolated to inclusive yields to previous results

p_T [GeV]	Asymmetry	Stat. unc.	Sys unc. (rel lumi vs. sqrt)	Sys unc. (from bg fraction unc)	Sys unc. (from bg asymmetry)	Sys unc. (total)
5 to 6	-0.000892	0.00296	6.47e-05	1.57e-05	0.00337	0.00337
6 to 8	0.00207	0.00401	1.77e-04	2.31e-05	0.00248	0.00249
8 to 10	0.00910	0.00806	7.45e-06	1.93e-04	0.00156	0.00157
10 to 18	0.00388	0.0105	7.48e-04	7.60e-05	7.67e-04	0.00107

Table 11: Final asymmetry summary table with statistical and systematic errors

7 Calculating Systematic Uncertainties and the Final TSSA Result

The final asymmetry values are shown in Figure 29 and summarized in Table 11. The central asymmetry value and statistical uncertainty come from the Relative Luminosity Formula result from Figure 23e. There are three sources of systematic uncertainty that are added in quadrature. The first is the difference between the Square Root and Relative Luminosity results in Figure 23e and listed in the middle column of Table 11

There is also a systematic uncertainty assigned because of the uncertainty on the background fraction. This was calculated by plugging in the uncertainty ranges on r from Tables 6 and 7 calculating how much that changed the overall asymmetry:

$$\frac{A_N^{iso}}{1-(r_{\pi^0} \pm \sigma_{r_{\pi^0}} \pm r_{merge}) - (r_\eta \pm \sigma_{r_\eta})} \tag{24}$$

These ranges were plugged in separately for the yellow left, yellow right, blue left, and blue right Relative Luminosity Formula results and then averaged together. The systematic uncertainty assigned was the maximum differences between these asymmetry values and the central Relative Luminosity asymmetry as a function of p_T. These values are listed in the middle column of Table 11.

The systematic uncertainty from setting the background asymmetry to zero was calculated in a similar manner: by plugging in a range for the background asymmetries and studying how much that changed the asymmetry value over all. The range that was used was the statistical uncertainty for the inclusive π^0 and η asymmetries integrated over photon p_T. Table 12 shows thee statistical uncertainties for the Relative Luminosity Formula from photons from π^0 and η pairs with $5 < p_T^\gamma < 18$ GeV. These $\sigma_{A_N^\eta}$ ranges were then plugged in separately for the yellow left, yellow right, blue left, and blue right Relative Luminosity Formula

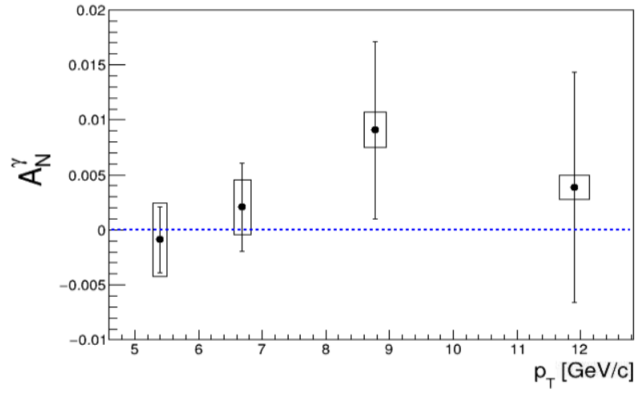

Figure 29: Final direct photon asymmetry with statistical and systematic errors

	$\sigma_{A_N^{\pi^0}}$	$\sigma_{A_N^{\eta}}$
Yellow Left	0.00327	0.00533
Yellow Right	0.00312	0.00496
Blue Left	0.00323	0.00514
Blue Right	0.00339	0.00552

Table 12: Ranges used for background asymmetries to calculate the systematic uncertainty from setting the background asymmetry to zero

results:

$$\frac{A_N^{iso} - r_{\pi^0}(0 \pm \sigma_{A_N^{\pi^0}}) - r_\eta(0 \pm \sigma_{A_N^{\eta}})}{1 - r_{\pi^0} - r_\eta} \tag{25}$$

and averaged together. The statistical uncertainty from setting the background asymmetry to zero was set to the difference between this shifted asymmetry and the central Relative Luminosity asymmetry values. These numbers a summarized in the second to last column in that table. Even though the ranges of the asymmetries that were plugged into the equation above do not change as a function of p_T, the background fraction does. At lower p_T there is a higher background fraction and so the uncertainty from the background asymmetry is larger. This uncertainty dominates the systematic uncertainty for most p_T bins.

A Good Run List

421716 421815 421816 421949 421961 421968 421969 421975 421976 421988 421989 421999 422014 422018 422020 422040 422041 422043 422045 422050 422051 422053 422054 422055 422057 422064 422066 422067 422068 422070 422074 422075 422084 422085 422123 422124 422135 422141 422147 422148 422200 422201 422202 422203 422205 422255 422256 422260 422262 422263 422266 422267 422268 422269 422272 422273 422298 422305 422314 422319 422322 422323 422324 422543 422553 422562 422566 422575 422611 422613 422614 422615 422618 422633 422640 422643 422756 422758 422762 422763 422779 422782 422785 423041 423043 423101 423109 423110 423132 423149 423220 423263 423268 423275 423278 423290 423301 423311 423377 423424 423432 423433 423546 423547 423548 423549 423550 423553 423576 423579 423632 423652 423663 423664 423676 423677 423679 423685 423696 423703 423820 423826 423828 423839 423843 423844 423845 423856 423860 423865 423867 423868 424038 424039 424040 424051 424052 424053 424055 424060 424061 424062 424063 424189 424190 424193 424194 424195 424255 424257 424270 424272 424273 424275 424276 424348 424353 424356 424358 424365 424368 424371 424372 424440 424441 424443 424444 424445 424452 424557 424584 424585 424626 424627 424629 424644 424671 424751 424753 424754 424755 424756 424759 424760 424761 424763 424817 424818 424827 424836 424878 424880 424881 424885 424886 425006 425008 425016 425078 425079 425080 425152 425168 425171 425172 425173 425212 425213 425214 425215

425287 425288 425289 425290 425292 425293 425294 425296 425377 425378 425395 425397 425409 425412 425413 425420 425422 425423 425424 425425 425428 425429 425431 425433 425434 425439 425553 425564 425566 425583 426112 426113 426114 426115 426116 426117 426252 426273 426281 426282 426283 426397 426401 426406 426407 426408 426409 426442 426443 426444 426445 426450 426460 426461 427013 427019 427020 427021 427024 427025 427026 427027 427111 427125 427135 427138 427141 427144 427145 427146 427147 427148 427149 427233 427239 427241 427243 427244 427262 427264 427360 427361 427362 427363 427366 427367 427373 427377 427380 427383 427384 427385 427388 427389 427390 427391 427393 427394 427397 427398 427481 427482 427483 427484 427485 427486 427498 427499 427500 427502 427508 427510 427514 427523 427527 427529 427530 427605 427654 427656 427657 427658 427660 427661 427662 427670 427671 427672 427673 427674 427708 427709 427710 427711 427712 427713 427805 427806 427807 427810 427811 427813 427814 427815 427829 427878 427879 427881 427882 427883 427885 427886 427887 427963 427964 427965 427966 427968 427970 427974 427975 427977 427979 427980 427982 427984 428166 428168 428169 428171 428204 428205 428206 428207 428208 428211 428212 428255 428256 428260 428261 428262 428263 428264 428266 428267 428268 428269 428272 428273 428318 428319 428321 428323 428324 428325 428326 428328 428329 428331 428377 428379 428381 428382 428384 428385 428386 428431 428432 428433 428446 428447 428448 428451 428452 428453 428454 428455 428459 428460 428601 428602 428603 428604 428605 428608 428609 428610 428613 428614 428615 428616 428617 428618 428710 428713 428714 428715 428728 428730 428733 428734 428735 428736 428737 428738 428739 428741 428754 428755 428757 428758 428759 428760 428762 428763 428771 428772 428891 428892 428893 428894 428896 428898 428929 428930 428931 428933 428934 429007 429010 429014 429016 429017 429022 429023 429024 429025 429026 429027 429029 429062 429066 429067 429068 429069 429070 429071 429112 429114 429115 429126 429127 429128 429129 429132 429133 429351 429352 429353 429355 429359 429361 429364 429365 429366 429368 429370 429504 429505 429506 429512 429518 429519 429549 429551 429552 429554 429555 429556 429589 429591 429592 429593 429594 429595 429596 429676 429678 429679 429680 429685 429686 429687 429688 429689 429691 429696 429787 429789 429795 429796 429797 429798 429799 429800 429801 429802 429886 429887 429888 429889 429890 429893 429894 429895 429896 429905 429906 429909 429910 429911 429912 429915 430013 430014 430016 430017 430022 430023 430024 430116 430117 430119 430120 430121 430123 430124 430125 430128 430131 430133 430134 430136 430141 430142 430143 430234 430235 430236 430237 430238 430239 430240 430241 430242 430277 430278 430279 430280 430281 430384 430386 430389 430390 430393 430402 430406 430407 430408 430409 430414 430415 430494 430496 430497 430500 430501 430502 430519 430520 430521 430522 430524 430525 430557 430558 430560 430562 430563 430565 430566 430594 430595 430596 430598 430599 430600 430606 430608 430676 430679 430680 430681 430682 430683 430692 430693 430694 430696 430697 430699 430700 430701 430702 430905 430906 430907 430909 430911 430912 430913 430914 430920 430921 430923 430924 430925 430927 430928 430929 430930 430931 430932 430933 430935 430936 431020 431021 431022 431023 431027 431028 431030 431031 431033 431036 431040 431122 431123 431125 431126 431127 431130 431131 431134 431135 431136 431137 431138 431139 431142 431143 431144 431145 431146 431147 431148 431149 431216 431217 431219 431220 431221 431224 431233 431234 431235 431239 431240 431256 431257 431258 431259 431260 431261 431294 431295 431298 431299 431301 431302 431357 431358 431360 431361 431362 431428 431429 431430 431432 431437 431447 431448 431453 431454 431458 431608 431609 431612 431615 431616 431618 431619 431620 431622 431717 431720 431725 431727 431731 431732 431733 431736 431738 431739 431744 431745 431746 431831 431833 431834 431835 431836 431837 431839 431840 431844 431845 431846 431859 431860 431886 431888 431889 431891 431892 431893 431894 431937 431938 431939 431940 431941 431942 431943 431948 431951 431959 431960 431963 431964 431997 432001 432002 432007

B Direct Photon Asymmetry Raw Counts and Asymmetry as a Function of Fill Group

Table 13 shows the total counts for direct photon candidates. Here the letters mean: U - spin up, D - spin down, L - left, R - right, Y - yellow beam asymmetry, B - blue beam asymmetry. The sum of all the counts for the yellow and blue beam match for each p_T bin. Figures 30– 33 show the asymmetry as a function of fill group index for direct photon candidates. As expected the calculated asymmetries are flat across the duration of Run 15, with no obvious dependence on spin pattern. Each of these plots are fit a constant, as shown on the plot, in order to calculate the weighted average of the asymmetry across all fill groups.

p_T[GeV]	ULY	DLY	URY	DRY	ULB	DLB	URB	DRB
5 - 6	208375	207178	201331	200625	200304	201652	207535	208018
6 - 8	86097	86178	83613	83696	83694	83615	85911	86364
8 - 10	15229	15205	14803	14927	14901	14829	15130	15304
10 - 18	6419	6447	6281	6224	6294	6211	6375	6491

Table 13: Total counts direct photon candidate counts

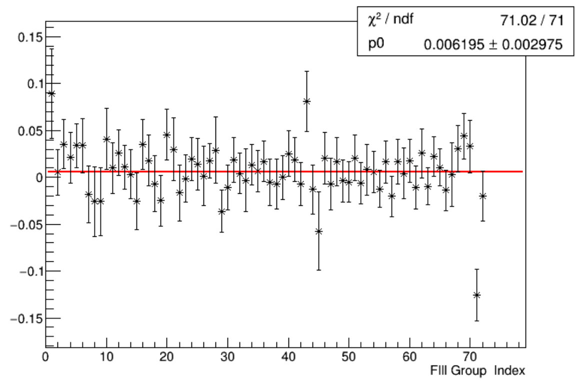

(a) Yellow Beam, Left Relative Luminosity Formula

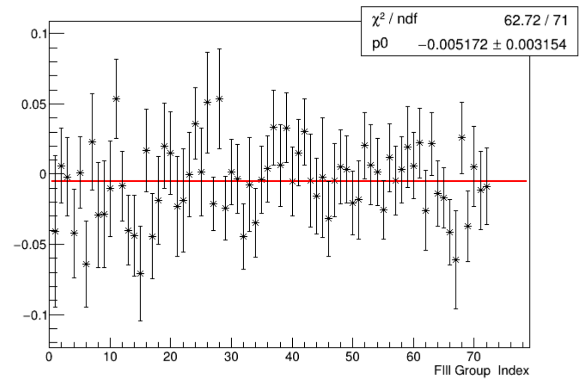

(b) Blue Beam, Left Relative Luminosity Formula

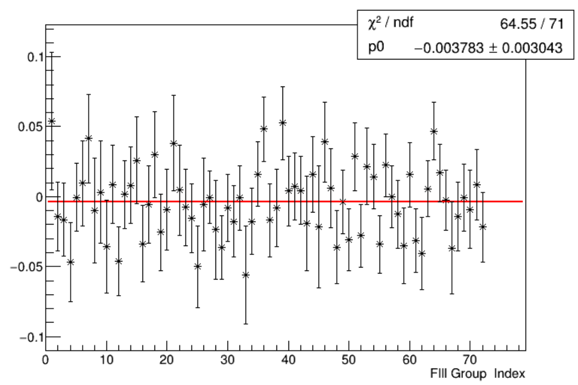

(c) Yellow Beam, Right Relative Luminosity Formula

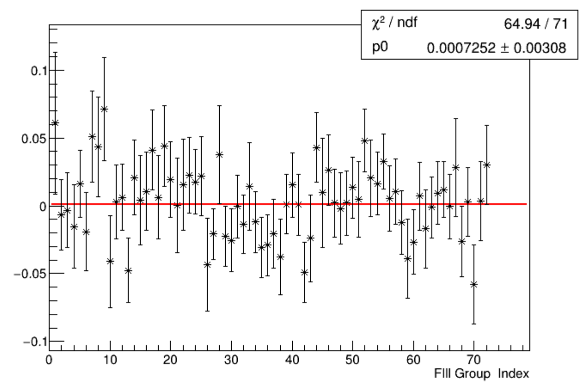

(d) Blue Beam, Right Relative Luminosity Formula

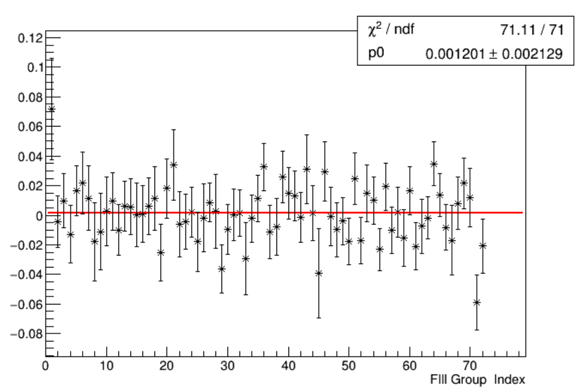

(e) Yellow Beam, Square Root Formula

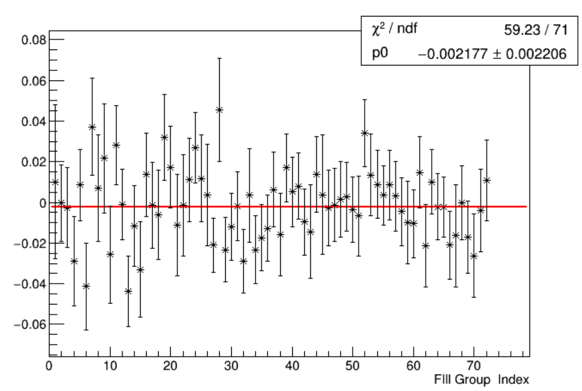

(f) Blue Beam, Square Root Formula

Figure 30: Asymmetry vs fill group for direct photon candidates with $5 < p_T < 6$ GeV

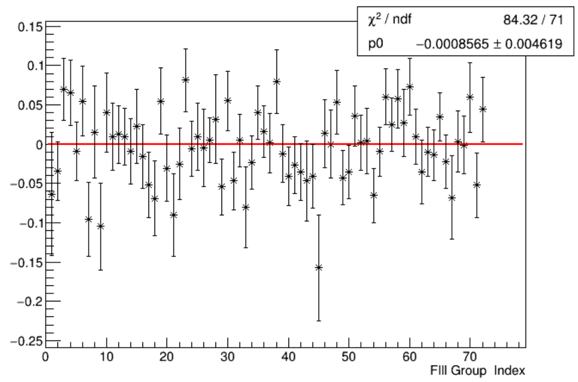

(a) Yellow Beam, Left Relative Luminosity Formula

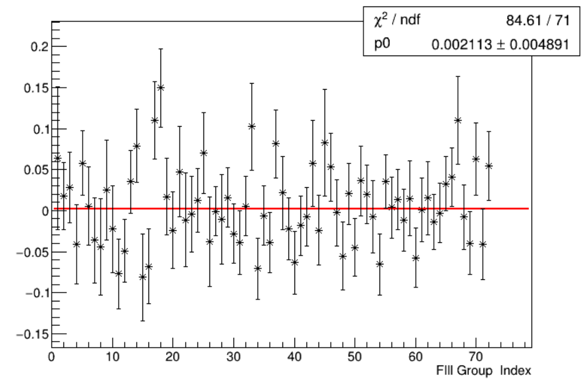

(b) Blue Beam, Left Relative Luminosity Formula

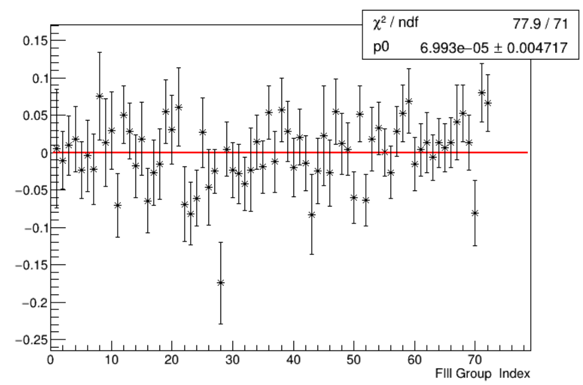

(c) Yellow Beam, Right Relative Luminosity Formula

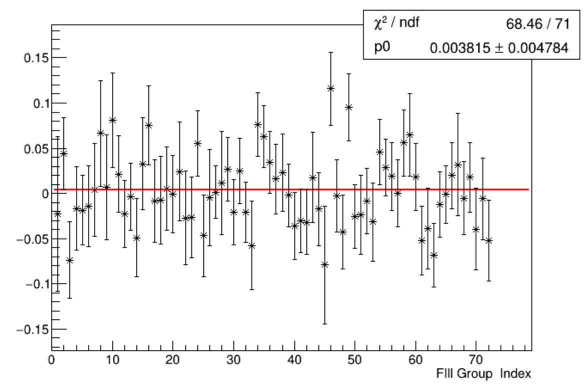

(d) Blue Beam, Right Relative Luminosity Formula

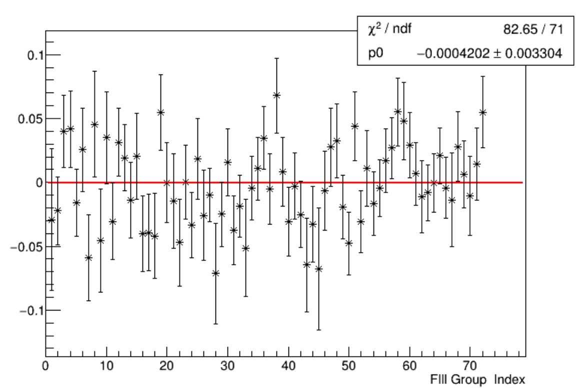

(e) Yellow Beam, Square Root Formula

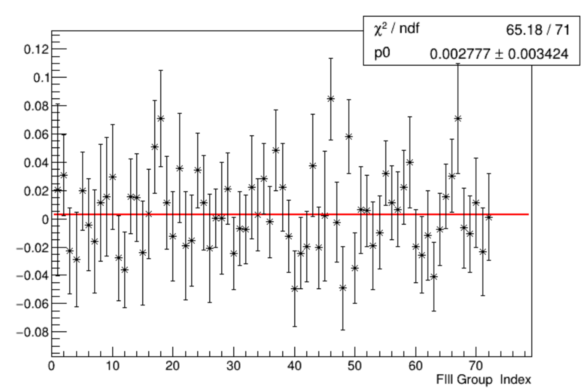

(f) Blue Beam, Square Root Formula

Figure 31: Asymmetry vs fill group for direct photon candidates with $6 < p_T < 8$ GeV

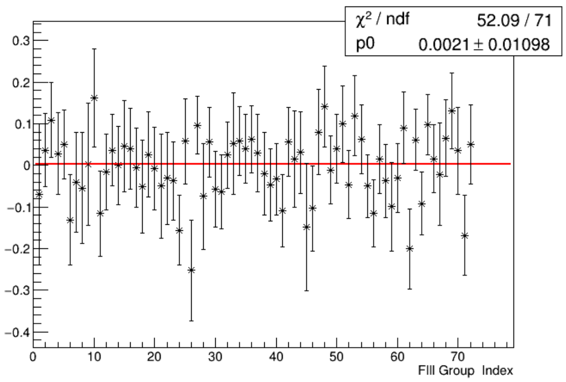

(a) Yellow Beam, Left Relative Luminosity Formula

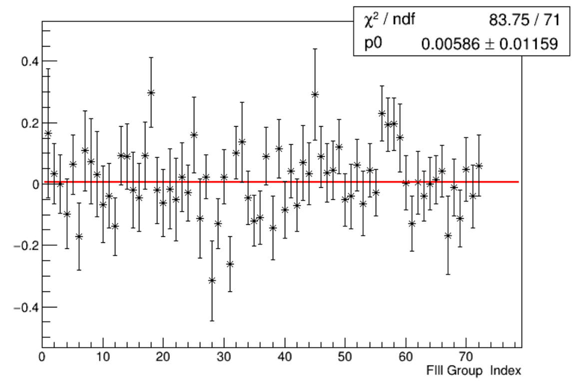

(b) Blue Beam, Left Relative Luminosity Formula

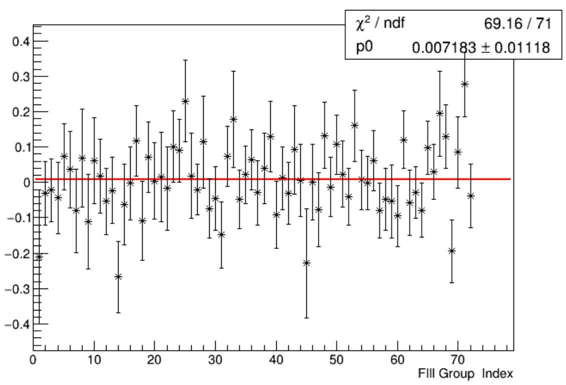

(c) Yellow Beam, Right Relative Luminosity Formula

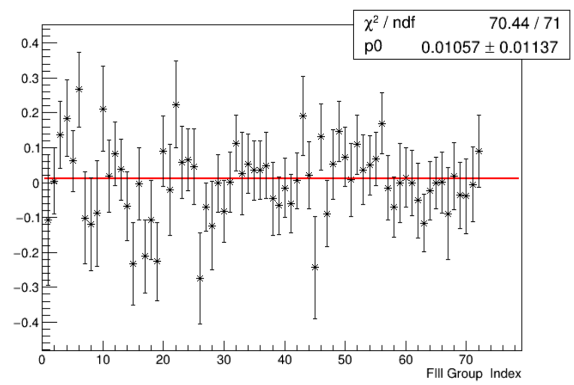

(d) Blue Beam, Right Relative Luminosity Formula

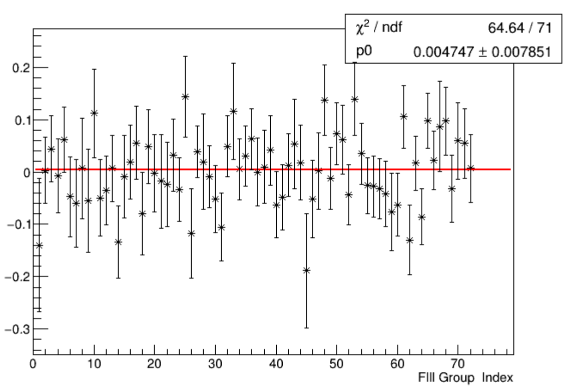

(e) Yellow Beam, Square Root Formula

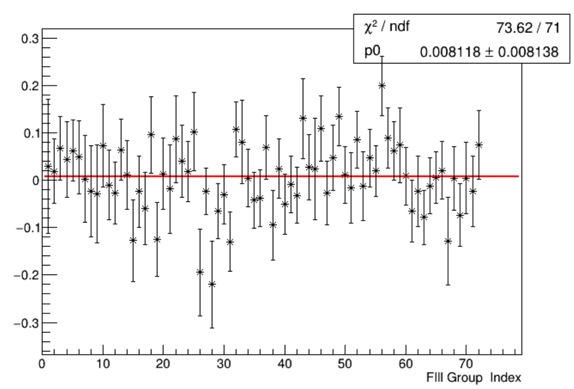

(f) Blue Beam, Square Root Formula

Figure 32: Asymmetry vs fill group for direct photon candidates with $8 < p_T < 10$ GeV

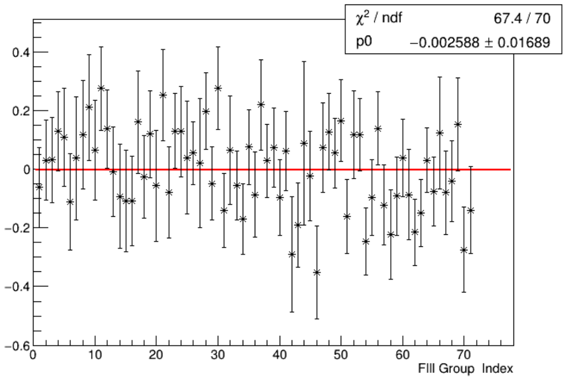

(a) Yellow Beam, Left Relative Luminosity Formula

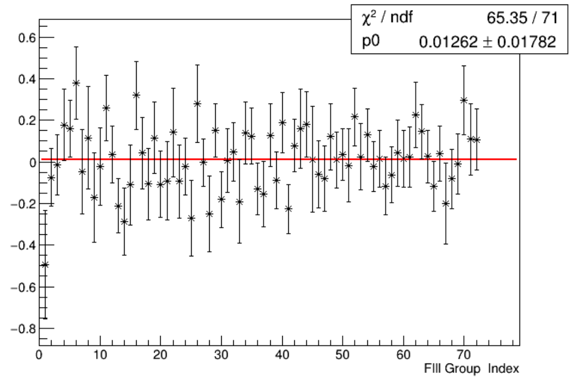

(b) Blue Beam, Left Relative Luminosity Formula

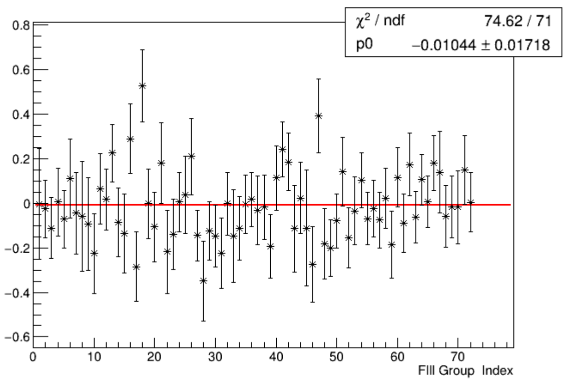

(c) Yellow Beam, Right Relative Luminosity Formula

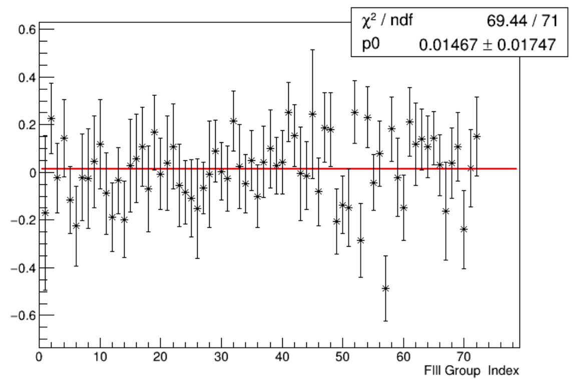

(d) Blue Beam, Right Relative Luminosity Formula

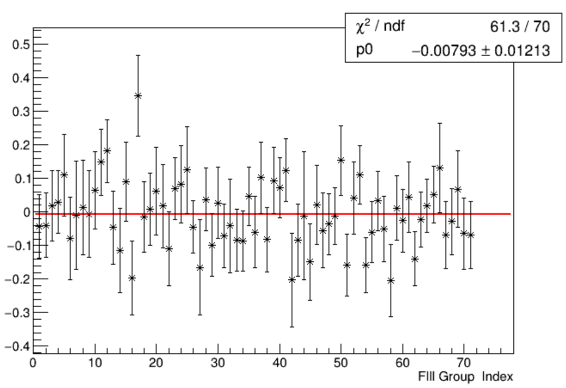

(e) Yellow Beam, Square Root Formula

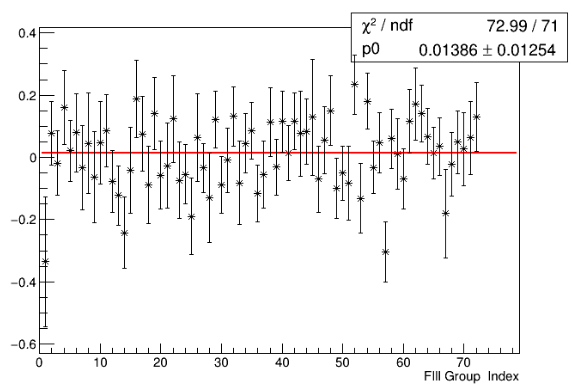

(f) Blue Beam, Square Root Formula

Figure 33: Asymmetry vs fill group for direct photon candidates with $10 < p_T < 18$ GeV